Biochemical Journal (2020) **477** 4491–4513
https://doi.org/10.1042/BCJ20200525

PORTLAND PRESS

Research Article

PARP-1 activation after oxidative insult promotes energy stress-dependent phosphorylation of YAP1 and reduces cell viability

Sandra M. Martín-Guerrero[1], Pedro Casado[2], Maruan Hijazi[2], Vinothini Rajeeve[2], Julio Plaza-Díaz[3,4], Francisco Abadía-Molina[1,5], Julio Navascués[1], Miguel A. Cuadros[1], Pedro R. Cutillas[2] and David Martín-Oliva[1]

[1]Departamento de Biología Celular, Facultad de Ciencias, Universidad de Granada, Spain; [2]Signalling and Proteomics Group, Centre for Genomics and Computational Biology, Barts Cancer Institute, Queen Mary University of London, London, U.K.; [3]Departamento de Bioquímica y Biología Molecular II, Facultad de Farmacia, Universidad de Granada, Granada, Spain; [4]Department of Pediatrics, Children's Hospital of Eastern Ontario Research Institute, Ottawa, Canada; [5]Instituto de Nutrición y Tecnología de los Alimentos 'José Mataix', Centro de Investigación Biomédica, Universidad de Granada, Granada, Spain

Correspondence: Sandra Maria Martín-Guerrero (sandra.martin_guerrero@kcl.ac.uk)

Poly(ADP-ribose) polymerase 1 (PARP-1) is a nuclear enzyme that catalyze the transfer of ADP-ribose units from NAD^+ to several target proteins involved in cellular stress responses. Using WRL68 (HeLa derivate) cells, we previously showed that PARP-1 activation induced by oxidative stress after H_2O_2 treatment lead to depletion of cellular NAD^+ and ATP, which promoted cell death. In this work, LC–MS/MS-based phosphoproteomics in WRL68 cells showed that the oxidative damage induced by H_2O_2 increased the phosphorylation of YAP1, a transcriptional co-activator involved in cell survival, and modified the phosphorylation of other proteins involved in transcription. Genetic or pharmacological inhibition of PARP-1 in H_2O_2-treated cells reduced YAP1 phosphorylation and degradation and increased cell viability. YAP1 silencing abrogated the protective effect of PARP-1 inhibition, indicating that YAP1 is important for the survival of WRL68 cells exposed to oxidative damage. Supplementation of NAD^+ also reduced YAP1 phosphorylation, suggesting that the loss of cellular NAD^+ caused by PARP-1 activation after oxidative treatment is responsible for the phosphorylation of YAP1. Finally, PARP-1 silencing after oxidative treatment diminished the activation of the metabolic sensor AMPK. Since NAD^+ supplementation reduced the phosphorylation of some AMPK substrates, we hypothesized that the loss of cellular NAD^+ after PARP-1 activation may induce an energy stress that activates AMPK. In summary, we showed a new crucial role of PARP-1 in the response to oxidative stress in which PARP-1 activation reduced cell viability by promoting the phosphorylation and degradation of YAP1 through a mechanism that involves the depletion of NAD^+.

Introduction

High levels of reactive oxygen species (ROS) are detrimental for cells because they damage several cell components including DNA, proteins and lipids [1]. Although organisms have developed an antioxidant system to regulate the production of ROS, an uncontrolled increase in ROS levels produces a harmful situation called oxidative stress [2]. In fact, high levels of ROS are associated with the pathology of multiple disorders [3].

Poly(ADP-ribose) polymerase 1 (PARP-1) can detect the presence of DNA damage generated by the action of ROS [4]. This protein is the founding member of the family of Poly(ADP-ribose) polymerases (PARPs), that add ADP-ribose units to target proteins [5,6]. PARP-1 attaches polymers of ADP-ribose (also referred as Poly-ADP-ribose or PAR) using NAD^+ as donor of ADP-ribose units in a process known as PARylation [5]. In addition to DNA damage detection and repair, PARP-1

Received: 29 June 2020
Revised: 26 October 2020
Accepted: 4 November 2020

Accepted Manuscript online: 4 November 2020
Version of Record published: 3 December 2020

Biochemical Journal (2020) 477 4491–4513
https://doi.org/10.1042/BCJ20200525

participates in other biological functions such as regulation of transcription, inflammation, cell cycle regulation and tumorigenesis [7]. PARP-1 activation can also trigger cell death processes. In fact, overactivation of PARP-1 after high levels of DNA damage depletes NAD^+, leading to cell death by energy depletion [8–11]. Furthermore, PARP-1 mediates a new type of cell death called *PARthanathos* [12]. In this case, PAR synthesized in the nucleus by PARP-1 migrates to the mitochondria, where it interacts with the apoptosis-inducing factor (AIF). This interaction promotes the translocation of AIF to the nucleus, which triggers cell death [12]. In addition, PARP-1 activity has been related with numerous disorders and diseases, which suggest that PARP-1 might be a potential target for the treatment of these diseases [7,13]. Specifically, in cancer cells with mutated DNA damage response genes or high levels of replicative stress, PARP-1 inhibitors destabilize the replication forks and induce further DNA damage and cell death [14,15]. Thus, the drug Olaparib and other PARP-1 inhibitors have been recently approved for cancer treatment. Defects in DNA repair lead to premature aging and DNA damage accumulates during aging. As cells age, PARP-1 activity increases as a consequence of the accumulation of DNA damage and repair, producing the depletion of NAD^+ levels, the alteration of cell metabolism and promoting the development of degenerative diseases [16], therefore, PARP-1 inhibitors could prevent, at least partially, these noxious effects [17]. Finally, the cell death called *PARthanatos*, associated to PARP-1 hyperactivation has been linked to neurodegenerative diseases [16,18]. In this sense, it has been described that PARP-1 inhibitors and NAD^+ precursors, increase NAD^+ levels, improve mitochondrial function and extent the live span of *Caenorhabditis elegans* [16,19].

The Hippo pathway, which is conserved from nematodes to humans, is involved in the control of a variety of cellular processes such as cell proliferation, apoptosis, organ size regulation and tissue regeneration [20]. This pathway comprises a cascade of kinases that phosphorylates the transcriptional co-activators YAP1 (yes-associated protein) and TAZ (transcriptional co-activator with PDZ-binding motifs) [21]. Phosphorylation of YAP1 after Hippo pathway activation promotes its cytoplasmic retention and degradation, reducing its interaction with the TEAD transcription factors and the expression of target genes [21–25]. The Hippo pathway is regulated by different signals such as cell–cell contact, cell polarity, energy stress, G-protein-coupled receptors (GPCRs) and cell cycle [26]. In fact, emerging evidence suggests a key role of the Hippo pathway in the response to multiple cellular stress types such as mechanical stress, DNA damage and oxidative stress [27]. In addition, it regulates the early stages of development; it is involved in the maintaining of cell quiescence in adult cells and promotes the regeneration of several tissues upon damage [28]. Therefore, the deregulation of this pathway may have negative consequences for the maintenance of cellular homeostasis, causing developmental defects, degenerative processes or tumorigenesis [27,29].

In a previous work, we demonstrated in human WRL68 cells that PARP-1 activation after oxidative treatment (with H_2O_2) increased cell death and mitochondrial fragmentation. In addition, pharmacological inhibition of PARP-1 or NAD^+ supplementation increased ATP levels and cell viability, while it reduced mitochondrial fragmentation and cell death [30]. In the present study, we used a label-free mass spectrometry-based phosphoproteomics approach to extend the role of PARP-1 under oxidative stress in WRL68 cells. We found that PARP-1 activation after oxidative treatment induced the phosphorylation of various proteins, including the transcriptional co-activator YAP1. Genetic and pharmacological inhibition of PARP-1 reduced the phosphorylation of YAP1 and increased the cell viability after oxidative treatment in a YAP1 dependent manner. Similarly, NAD^+ supplementation reduced the phosphorylation of YAP1 after the oxidative insult, indicating that the depletion of NAD^+ levels after PARP-1 activation might be responsible for YAP1 phosphorylation. In summary, our findings suggest that PARP-1 activation after oxidative treatment depletes NAD^+ levels and induces an energy stress, which promotes the phosphorylation and degradation of YAP1, a transcriptional co-activator relevant for the viability of WRL68 cells under oxidative insult.

Materials and methods

Cell culture and treatments

Human WRL68 cells (HeLa derivative cell line) were purchased by the Scientific Instrumentation Services (CIC) of the University of Granada from the European Collection of Authenticated Cell Cultures (cat # 89121403). WRL68 cells were cultured in DMEM medium (Sigma/Gibco) with 10% foetal bovine serum (FBS, Sigma/Gibco) and L-glutamine solution (2 mM, Sigma) containing streptomycin (100 µg/ml) and penicillin (100 U/ml). Oxidative insult was achieved by treating WRL68 cells with a single dose of H_2O_2 (from a 30% stock solution, Sigma) diluted to 3.5 mM in the medium for 30 min. After 30 min, the medium was replaced

with fresh growth medium (without H_2O_2), and the cells were further incubated (post-treatment incubation) for 2 h for phosphoproteomics analysis; 0, 2, 4, 6 and 12 h for western blot assays or 24 h for viability assays.

The PARP-1 inhibitor PJ34 (cat # ALX-270-289, Enzo Life Sciences or cat # S7300, Selleckchem) was used at a final concentration of 1 μM. Cells were incubated with PJ34 for 16 h prior to H_2O_2 treatment and the inhibitor was maintained during H_2O_2 treatment and post-treatment incubation. To avoid NAD^+ depletion, exogenous NAD^+ (250 μM, Sigma) was added to the cell culture during the H_2O_2 treatment and to the fresh medium during post-treatment incubation.

Silencing of PARP-1 or YAP1 using siRNA

On-TARGET Plus Smart pool siRNA targeting human PARP-1 and human YAP1 were purchased from Dharmacon (cat # L-006656-03-0005 and cat # L-012200-00-0005, respectively). ON-TARGET Plus Non-targeting Control Pool was used as a negative control of transfection (cat # D-001810-10-05, Dharmacon). Cells were transfected with siRNAs (final concentration of 50 nM) using Lipofectamine 3000 (Invitrogen) for 72 h in reduced serum medium Opti-MEM™ (Gibco). After transfection, cells were treated with H_2O_2 (3.5 mM) as indicated in the previous section.

Cell viability assays

Cell viability was determined using the MTS (3-[4,5-dimethylthiazol-2-yl]-2,5-diphenyl tetrazolium bromide, Sigma) method. Cells were incubated with MTS at 37°C in 5% CO_2 and the absorbance at 490 nm of each well was measured every 10 min until the saturation of the reaction in a microplate spectrophotometer reader (Microplate Readers FLUOstar® Omega, BMG LABTECH). All the absorbances values were corrected to the background signal. Cell viability was expressed as a percentage in relation to the control cells (H_2O_2 non-treated cells), that represented 100% viability.

Sulforhodamine B (SRB) assay

SRB staining was used to determine the effect of H_2O_2 treatment and PARP-1 inhibition on cell proliferation. Cells were seeded on 96-well plates, incubated with H_2O_2 as described in previous sections and left to recover for 48 h with or without PJ34 inhibitor. Cells were fixed in an ice-cold solution of 10% tri-chloro acetic acid (Sigma) and stained with SRB following the protocol described in [31]. Finally, optic density (OD) was measured at 492 nm in a microplate spectrophotometer reader (Multiskan Ascent, Thermo Scientific), and cell proliferation was expressed as a percentage in relation to control cells (H_2O_2 non-treated cells), that represented 100%.

Determination of γH2AX in WRL68 cells

Accumulation of DNA damage was evaluated by the immunostaining of the phosphorylated form of histone H2AX in Ser139 (γH2AX). WRL68 cells were seeded on coverslips in 6-well plates, treated for 30 min with H_2O_2 and post-incubated with fresh medium for 2 and 4 h. Then, cells were fixed with 4% paraformaldehyde (PFA) for 30 min at room temperature, permeabilized with 0.2% Triton X100 in PBS and blocked with blocking solution (3% bovine serum albumin in PBS with 0.1% Tween-20) for 1 h at RT. Then, coverslips were incubated overnight at 4°C with anti-γH2AX (pS139) antibody (dilution 1 : 500, cat # 560443, BD Pharmigen) in blocking solution, and then with the secondary antibody Alexa fluor 594-conjugated goat anti-mouse IgG (dilution 1 : 1000, cat # A-11005, Molecular Probes) in blocking solution at room temperature for 2 h. Finally, nuclei were counterstained with DAPI (1 μg/ml, Sigma) and mounted with Fluoromount G mounting medium (Southern Biotech). Confocal images were obtained with a TCS-SP5 microscope (Leica) using a 63X objective. Images were stored in tagged image file format and digitally prepared by automatically adjusting their brightness and contrast.

For quantitative studies, the percentage of γH2AX-positive cells was determined by flow cytometry. WRL68 cells were seeded in 6-well plates, treated with H_2O_2 and post-incubated in fresh medium for 4 h, as previously described. Cells were recovered by trypsinization, washed twice with ice-cold PBS and fixed in 4% PFA for 30 min at room temperature. Then, cells were washed with PBS and left overnight with a solution of 1% bovine serum albumin in PBS with 0.1% Tween-20. The following day, cells were resuspended in BD Perm/Wash™ Buffer 1x (cat # 554714, BD Cytofix/Cytoperm™) and incubated for 15 min at room temperature. Finally, 5 μl of PE-CF594 Mouse anti-H2AX (pS139) (dilution 1 : 20, cat # 564719, BD Horizon) were added and cells were incubated in this solution for 30 min at room temperature. The percentage of γH2AX-positive cells was analyzed with a BD FACSARIA II cytometer using BD FACSDIVA™ 6.0 software (BD Biosciences).

PORTLAND PRESS

Biochemical Journal (2020) 477 4491–4513
https://doi.org/10.1042/BCJ20200525

Sample preparation, phosphopeptide enrichment and LC–MS/MS detection

Phosphoproteomics studies were performed using liquid chromatography tandem-mass spectrometry (LC–MS/MS). WRL68 cells were treated with H_2O_2 for 30 min, post-incubated in fresh medium for 2 h and processed for phosphoproteomics analysis following the protocol described in [32,33]. In the assays using PJ34 inhibitor or NAD^+ supplementation, cells from four independent experiments were lysed in urea buffer containing phosphatase inhibitors and 500 μg of extracted proteins were digested using trypsin as described in [33]. In siRNA experiments, cells from four independent experiments were lysed in urea buffer containing phosphatase inhibitors and 80 μg of extracted proteins were digested using trypsin as described in [33]. Following the digestion, the samples were subjected to desalting, and phosphopeptides were enriched using TiO_2 as described in [33]. In the case of siRNA samples, the desalting was performed using C18 + GC carbon tips (TopTip with Filter C18 + Carbon 10–200 μl, cat # TF2MC18.96, Glygen) as described in [34] with the exception of the elution step that was done with 1 M glycolic acid in 50% acetonitrile (ACN) and 5% trifluoroacetic acid (TFA). Then, the enrichment of phosphopeptides was performed as in [33].

Finally, dried phosphopeptides pellets were resuspended in reconstitution buffer (20 fmol/μl enolase in 3% ACN, 0.1% TFA) and loaded in an LC–MS/MS platform consisting in a DionexUltiMate 3000 RSLC coupled to an Orbitrap Q-Exactive Plus mass spectrometer with an Easy Spray ionization system (ThermoFisher Scientific). The phosphopeptides were first trapped in a trapping column for 3 min with a flow rate of 0.25 μl/min (LC AcclaimTM PepMapTM 100 C18 LC 300 μm x 5 mm, ThermoFisher Scientific) and then, separated using a 3–23% ACN gradient for 90 min with a flow rate of 0.25 μl/min in an analytic column (Easy Spray RSLC C18 2 μm 50 cm × 75 μm, ThermoFisher Scientific). Samples were run in the LC–MS/MS system in a randomized manner by shuffling samples before loading (samples were run twice for assays using PJ34 inhibitor or NAD^+, and once for siRNA assays). Acquisition of full scan survey spectra (m/z 375–1500) was followed by data-dependent acquisition in which the 15 most intense ions were selected for HCD (higher-energy collisional dissociation) and MS/MS scanning. A 30 s dynamic exclusion period was enabled with an exclusion list with 10 ppm mass window.

Identification and quantification of phosphopeptides and phosphorylation sites

Mascot Daemon was used to automate the identification of phosphopeptides. Thus, Mascot Distiller was used to generate the peak lists that were loaded into the Mascot Search Engine (v2.5). Searches were performed against the Swiss-Prot Human database (uniprot_sprot_2014_08.fasta) considering 2 trypsin missed cleavages, a mass tolerance of ±10 ppm for the MS scans and ±25 mmu for the MS/MS scans. Carbamidomethyl Cys was set as a fixed modification while PyroGlu on N-terminal Gln, oxidation of Met and phosphorylation on Ser, Thr and Tyr were considered as variable modifications [35]. Pescal software was used for the label-free quantification of phosphopeptides [32]. XICs for all the peptides identified were constructed across all samples with ±7 ppm and ±2 min mass and retention time windows, respectively. Peak areas from all XICs were calculated. Undetectable data points for a certain peptide were given the intensity value of 1/10 of minimal intensity detected for that peptide across all the samples. For each sample, intensity values were normalized to the sum of all peptide intensities derived from that sample. To determine phosphorylation changes induced by treatments, the normalized signals from treated cells were divided by those of the reference sample (control or H_2O_2 treatment) and given as Log2 of Fold Changes. The data obtained after identification and quantification is provided in Supplementary Dataset S1.

Bioinformatic analysis of quantitative mass spectrometry data

Two tail unpaired Student's t-test was used to determine significance values (values indicated in Supplementary Dataset S1). Phosphopeptides showing a significant difference ($P \leq 0.05$) with a Log2 Fold Change ≥ 1 (increased phosphorylation) or ≤ -1 (decreased phosphorylation) in the comparison of interest were used for further analyses. Thus, one-way analysis of variance (ANOVA) followed by Tukey's Multiple Comparison Tests was used in detailed analyses shown in dot plots.

Inference of kinase activities from the phosphoproteomics data was performed using kinase substrate enrichment analysis (KSEA) as described [36]. KSEA estimates the activity of a given kinase based on the phosphorylation of substrates linked to that particular kinase. Only kinase activities in which KSEA score was calculated with five or more substrates were considered.

Heatmaps and Venn diagrams were elaborated using the online tools *Heatmapper* [37] and *Venny 2.1* (http://bioinfogp.cnb.csic.es/tools/venny/index.html). Volcano plots were generated in an R environment (RStudio) using the ggplot package. Dot and bar plots were generated using GraphPad Prism.

Gene ontology (GO) analysis of genes from phosphoproteomics data was performed using David Bionformatics Resources 6.8 [38] using the human genome as background dataset. Phosphopeptides with a significant ($P \leq 0.05$) Log2 Fold Change higher than 1 or lower than −1 compared with the control cells were subjected to GO analysis. The threshold value of group membership counts was set at 2 and the EASE score (modified Fisher's exact *P*-value) was set at 0.05. The first 10 significant GO terms to 'Biological Process' with larger number of genes were represented.

Western blot

Cells were scraped in RIPA buffer containing phosphatase inhibitors (1 mM NaF and 1 mM Na_3VO_4) and a protease inhibitor cocktail (cat # P8340, SIGMA). Afterwards, proteins were separated in 4–12% Bis-Tris Midi Protein Gels (NuPAGE™ 4–12% Bis-Tris Midi Protein Gels, cat # WG1402BOX, ThermoFisher Scientific) and transferred onto nitrocellulose membranes (iBlot™ Transfer Stack, nitrocellulose, regular size, cat # IB301001, ThermoFisher Scientific). Then, blots were blocked in 10% (w/v) Skim milk (cat # 70166, Sigma) in TBS/T (tris-buffered saline with 0.1% Tween-20) for 30 min and incubated (4°C, overnight) with primary antibody solution (in 5% [w/v] skim milk in TBS/T). Membranes where washed with TBS/T and incubated with the corresponding peroxidase-conjugated secondary antibody solution (in 5% [w/v] skim milk in TBS/T) during 2 h at room temperature. The antibody reaction was documented with the Amersham Imager 600RGB Chemidoc using a chemiluminescence reagent (SuperSignal™ West Pico PLUS Chemiluminescent Substrate, cat # 34080, ThermoFisher Scientific). Primary antibodies were directed against human PARP-1 (dilution 1 : 1000, cat # 556362, BD Pharmingen) and human YAP1 (dilution 1 : 1000, cat # sc-101199, Santa Cruz Biotechnology). Primary antibody anti-β-actin (dilution 1 : 1000; cat # 8457, Santa Cruz Biotechnology) was used to control equal loading of protein and western blot normalization. Anti-rabbit IgG or anti-mouse IgG antibodies conjugated to horseradish peroxidase (dilution 1 : 5000; cat # 7076S from Cell Signaling, and cat # NA934-1ML from GE healthcare) were used as secondary antibodies. Western blot quantification was performed using Image Studio™ Lite Software (LI-COR Biosciences). Signal intensity was normalized to β-actin signal, and the level of protein was expressed as relative level to control.

Statistical analysis

Data were expressed as mean ± SEM from at least three independent experiments. ANOVA with Tukey's Multiple Comparison Tests were used to determine significant differences in MTS assays. Significant differences were determined with the Student's *t*-test if it is not specified. The statistical analyses were performed using GraphPad Prism and Microsoft Office Excel. A value of $P \leq 0.05$ was considered statistically significant.

Results

The oxidative treatment with H_2O_2 modified the phosphoproteome of the human WRL68 cells

Changes in the pattern of protein phosphorylation of WRL68 cells under oxidative stress were evaluated performing LC–MS/MS. The oxidative stress was generated by 30 min treatment with H_2O_2, followed by an additional post-incubation time of 2 h in medium supplemented with the PARP-1 inhibitor PJ34 or NAD^+ as indicated in Figure 1A. Finally, the samples were processed for phosphoproteomics analysis (Figure 1B and Supplementary Dataset S1).

H_2O_2 treatment increased significantly the phosphorylation of 1377 peptides ($P \leq 0.05$; Log2 Fold Change ≥ 1, red dots in Figure 2A, left diagram) and decreased significantly the phosphorylation of 717 peptides ($P \leq 0.05$; Log2 Fold Change ≤ −1, blue dots in Figure 2A, left diagram) relative to H_2O_2 non-treated cells (control).

PARP-1 inhibition or NAD^+ supplementation modified the phosphorylation pattern induced by the oxidative treatment

We have shown that in WRL68 cells PARP-1 inhibition restored cell viability and decreased cell death 24 h after 30 min exposure to 3.5 mM H_2O_2 treatment ([30]), and also increased cell proliferation after 48 h of oxidative treatment (Supplementary Figure S1). We also demonstrated that 3.5 mM was the lowest concentration

Biochemical Journal (2020) 477 4491–4513
https://doi.org/10.1042/BCJ20200525

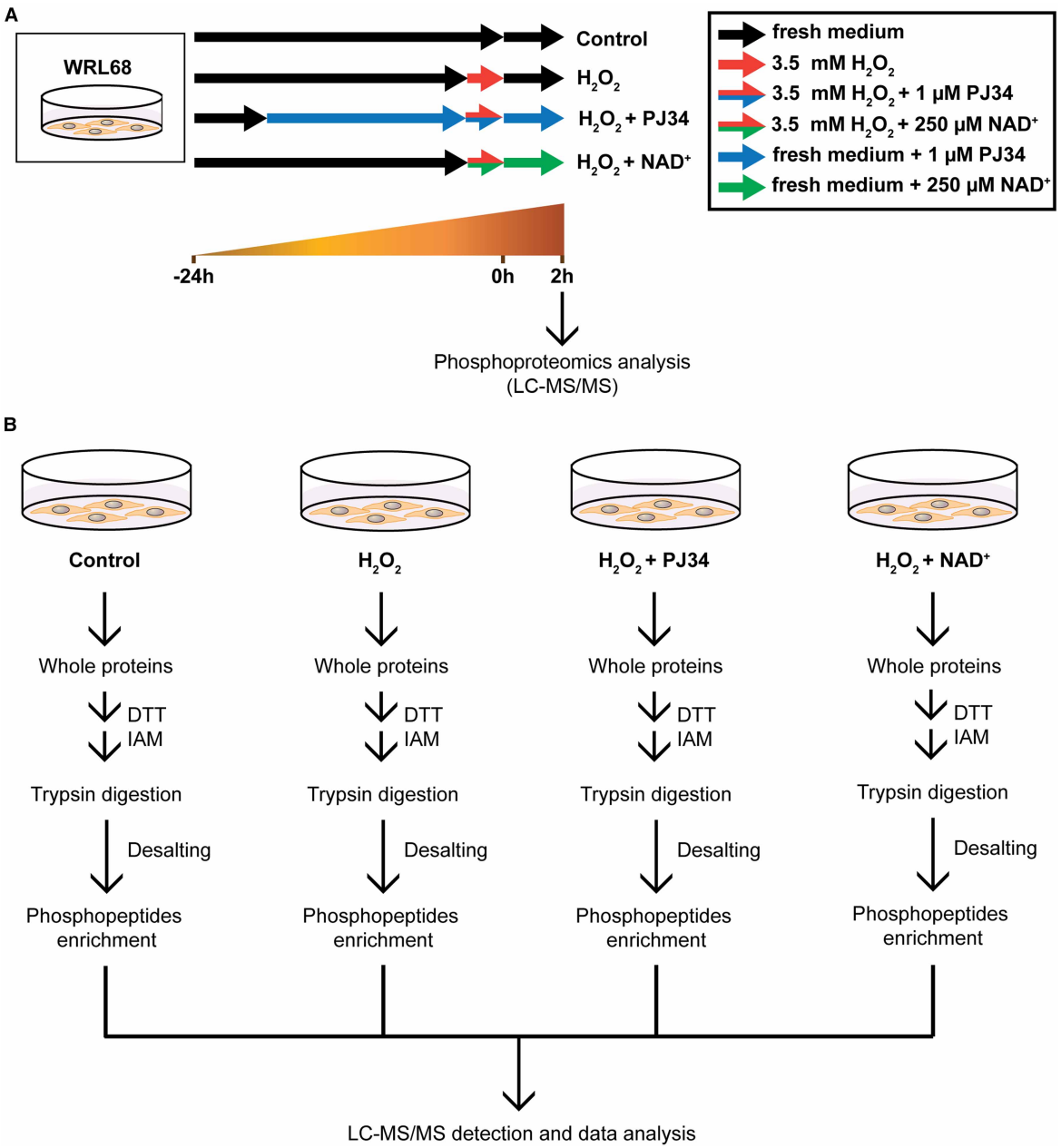

Figure 1. Experimental workflow.

(**A**) A single dose of H_2O_2 (3.5 mM) for 30 min was used to induce oxidative stress in WRL68 cells. After H_2O_2 exposure, the medium was replaced, and the cells were further incubated in fresh medium (without H_2O_2) for 2 h (post-treatment incubation). PARP-1 inhibitor PJ34 (1 μM) was added 16 h prior to oxidative treatment and was maintained all the time. Media were supplemented with NAD^+ (250 μM) during H_2O_2 treatment and during post-treatment incubation. (**B**) At the end of the post-treatment incubation, cells were lysed, and the extracted proteins were processed for LC–MS/MS analysis. For that purpose, proteins were reduced with DTT, alkylated with iodoacetamide (IAM) and digested with trypsin. Peptides were desalted and phosphopeptides were enriched using TiO_2 and analyzed by mass spectrometry techniques (LC–MS/MS). Four independent biological replicates for each condition were performed.

Biochemical Journal (2020) **477** 4491–4513
https://doi.org/10.1042/BCJ20200525

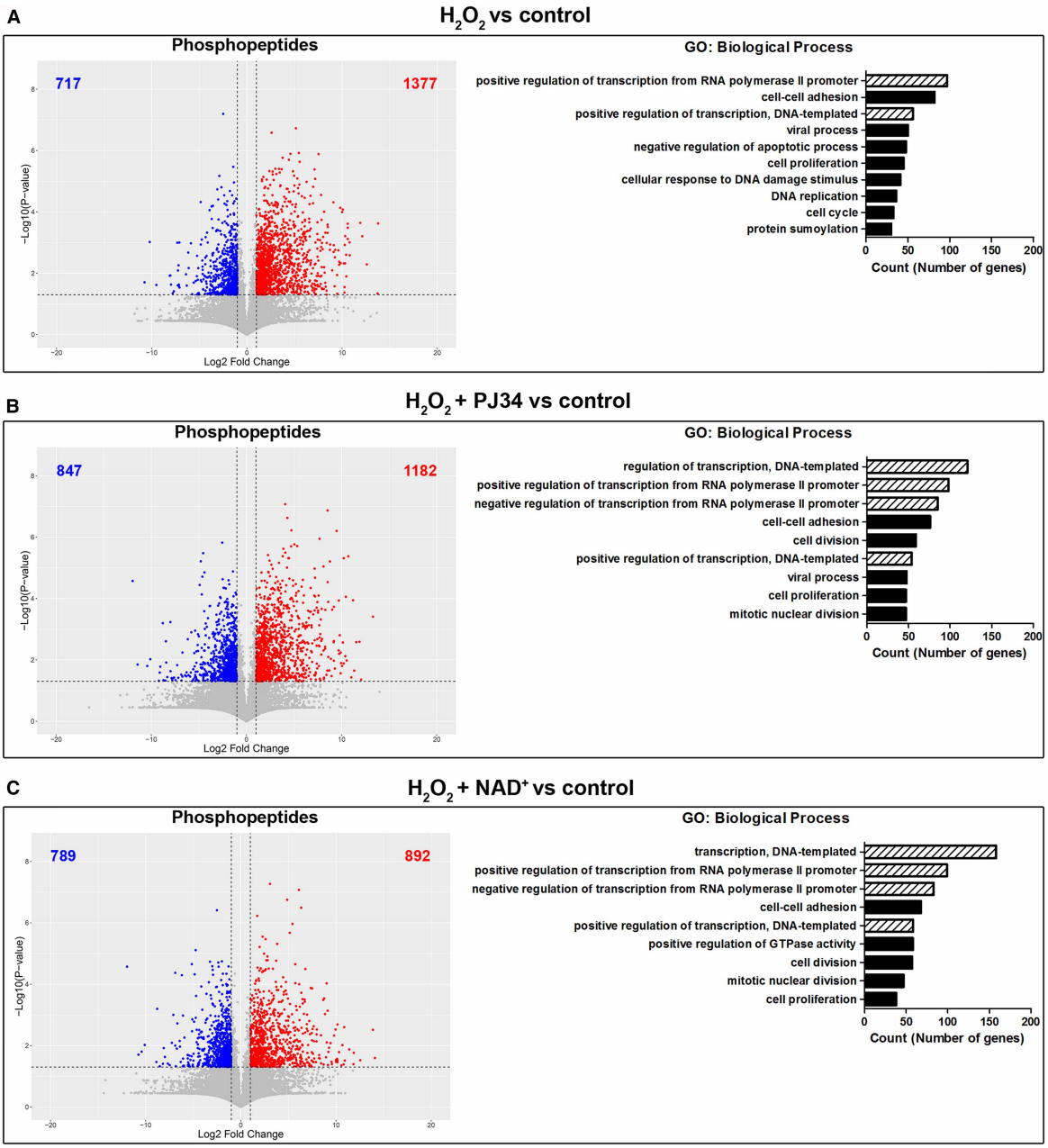

Figure 2. Overview of H_2O_2 effects in the absence or presence of the PARP-1 inhibitor PJ34 or NAD^+ supplementation on the phosphoproteome of WRL68 cells and its linked GOs. Part 1 of 2

(**A**) Volcano plot (left image) showing the phosphopeptides identified by LC–MS/MS analysis in WRL68 cells after H_2O_2 treatment. The *x*-axis represents the degree of phosphorylation (referred as Log2 Fold Change) relative to control cells (H_2O_2 non-treated cells), and the *y*-axis shows their statistical significance (–Log10 *P*-value). Horizontal and vertical dashed lines indicate the filtering criteria (*P*-value = 0.05 and Log2 Fold Change = ±1.0, respectively). Red and blue dots correspond to phosphopeptides that changed significantly in experimental conditions respect to control ($P \leq 0.05$, Log2 Fold Change ≥ 1 and Log2 Fold Change ≤ -1, respectively), while grey dots represent phosphopeptides that did not match with the filtering criteria ($P \geq 0.05$, Log2 Fold Change > -1 or Log2 Fold Change < 1). Blue and red numbers represent the number of phosphopeptides with significant decreased (Log2 Fold Change ≤ -1, $P \leq 0.05$) and increased (Log2 Fold Change ≥ 1, $P \leq 0.05$) phosphorylation, respectively. Right image shows DAVID Bioinformatics analysis to determine GO enrichment for Biological Process terms from significant modified phosphopeptides (red and blue dots from volcano plot). Each bar graph represents the number of genes corresponding to each term; only the 10 most populated terms (significant terms associated with more genes) are represented.

Biochemical Journal (2020) **477** 4491–4513
https://doi.org/10.1042/BCJ20200525

Figure 2. Overview of H_2O_2 effects in the absence or presence of the PARP-1 inhibitor PJ34 or NAD^+ supplementation on the phosphoproteome of WRL68 cells and its linked GOs. Part 2 of 2

The bars chart with diagonal stripes highlights the GO terms related with transcription processes. In (**B**,**C**) are represented the volcano plots (left images) and the GO analysis (right images) for cells treated with H_2O_2 + PJ34 (**B**) and H_2O_2 + NAD^+ (**C**), respectively.

of H_2O_2 able to generate enough ROS to trigger the hyperactivation of PARP-1 in our WRL68 model [30]. In addition, immunofluorescence imaging and flow cytometry data on γH2AX suggested that PARP-1 inhibition reduced the DNA damage induced by H_2O_2 4 h after treatment (Supplementary Figure S2). To study the kinase signalling associated to PARP-1 activation under these conditions, we analyzed protein phosphorylation in WRL68 cells subjected to treatment with H_2O_2 in the presence of the PARP-1 inhibitor PJ34 (H_2O_2 + PJ34 treatment). In this case, 1182 peptides showed a significant increased phosphorylation ($P \leq 0.05$; Log2 Fold Change ≥ 1, red dots in Figure 2B, left diagram), while 847 peptides showed a significant decreased phosphorylation ($P \leq 0.05$; Log2 Fold Change ≤ -1, blue dots in Figure 2B, left diagram) both relative to control cells. Interestingly, this analysis suggested that PARP-1 inhibition changed the pattern of phosphorylation since it reduced the number of peptides with increased phosphorylation and increased those with reduced phosphorylation (compare the upper left and right quadrants in volcano plots of Figure 2A,B). Since supplementation with 250 μM NAD^+ (substrate of PARP-1) increased ATP levels and showed the same protective effect over cell viability as the PJ34 inhibitor in WRL68 cells [30], we investigated whether NAD^+ supplementation could also have an impact on the phosphoproteome of WRL68 cells treated with H_2O_2. In fact, NAD^+ supplementation showed the smallest number of peptides with increased phosphorylation compared with the other conditions (red dots in Figure 2C, left diagram; compare the upper right quadrants in volcano plots of Figure 2A–C). At the same time, this treatment slightly altered the number of peptides with decreased phosphorylation when compared with H_2O_2 treatment alone (compare the upper left quadrants in volcano plots of Figure 2A,C). These results suggested that either PJ34 inhibitor or NAD^+ supplementation affected the phosphorylation pattern induced by the oxidative insult.

To further analyze the biological process to which those peptides contribute, we subjected the differentially regulated phosphopeptides in each treatment to GO analysis using the DAVID bioinformatics tool [38]. In the bar plots of Figure 2, we represented the 10 most relevant terms linked to the aspect 'Biological Process' in each treatment (significant terms with the largest number of genes). The most populated terms were preferentially associated with transcription processes (Figure 2, diagonal stripe bars). Of note, the number of terms related to transcription processes and the number of genes in those terms increased when PARP-1 was inhibited or NAD^+ was added (compare the bar graphs in Figure 2). These results suggest that the modified peptides in our treatments contributed to transcription processes (Figure 2).

To further study the effect of PARP-1 inhibition or NAD^+ supplementation in the phosphoproteome of cells under oxidative stress, we selected the phosphopeptides significantly affected by H_2O_2 treatment (H_2O_2 vs control) and we determined the significantly modified peptides in 'H_2O_2 + PJ34' or 'H_2O_2 + NAD^+' treatments compared with 'H_2O_2' treatment. PARP-1 inhibition and NAD^+ supplementation significantly increased the phosphorylation of 5 and 27 peptides and decreased the phosphorylation of 71 and 54 peptides, respectively (Figure 3A). In common, both treatments increased the phosphorylation of 1 peptide and decreased the phosphorylation of 17 peptides (Figure 3A,B). The phosphorylation levels of the common peptides for each comparison are represented in Figure 3C. Taken together, these results suggest that PARP-1 inhibition or NAD^+ supplementation in H_2O_2-treated cells mainly reduced the phosphorylation of proteins induced by the oxidative treatment.

We observed that H_2O_2 treatment significantly increased the phosphorylation of the transcriptional co-activator YAP1, the final effector of the Hippo pathway, at Ser397 and Ser400 (Figure 3D, black dots versus red triangles). Of note, PARP-1 inhibition or NAD^+ supplementation in cells under oxidative stress significantly reduced the phosphorylation of YAP1 at those residues similar to the levels of control cells (Figure 3D, red triangles versus green squares or orange dots). We also detected an increased YAP1 phosphorylation at other sites after H_2O_2 treatment (Figure 3E). The phosphorylation of YAP1 peptides containing Thr376 or Ser127 and Ser128 was also significantly reduced when PARP-1 was inhibited while NAD^+ supplementation followed the same trend (Figure 3E). In the case of a YAP1 peptide containing Thr141, Thr143 and Thr145, the phosphorylation was significantly reduced when NAD^+ was supplemented while PARP-1 inhibition followed the same trend (Figure 3E).

Biochemical Journal (2020) **477** 4491–4513
https://doi.org/10.1042/BCJ20200525

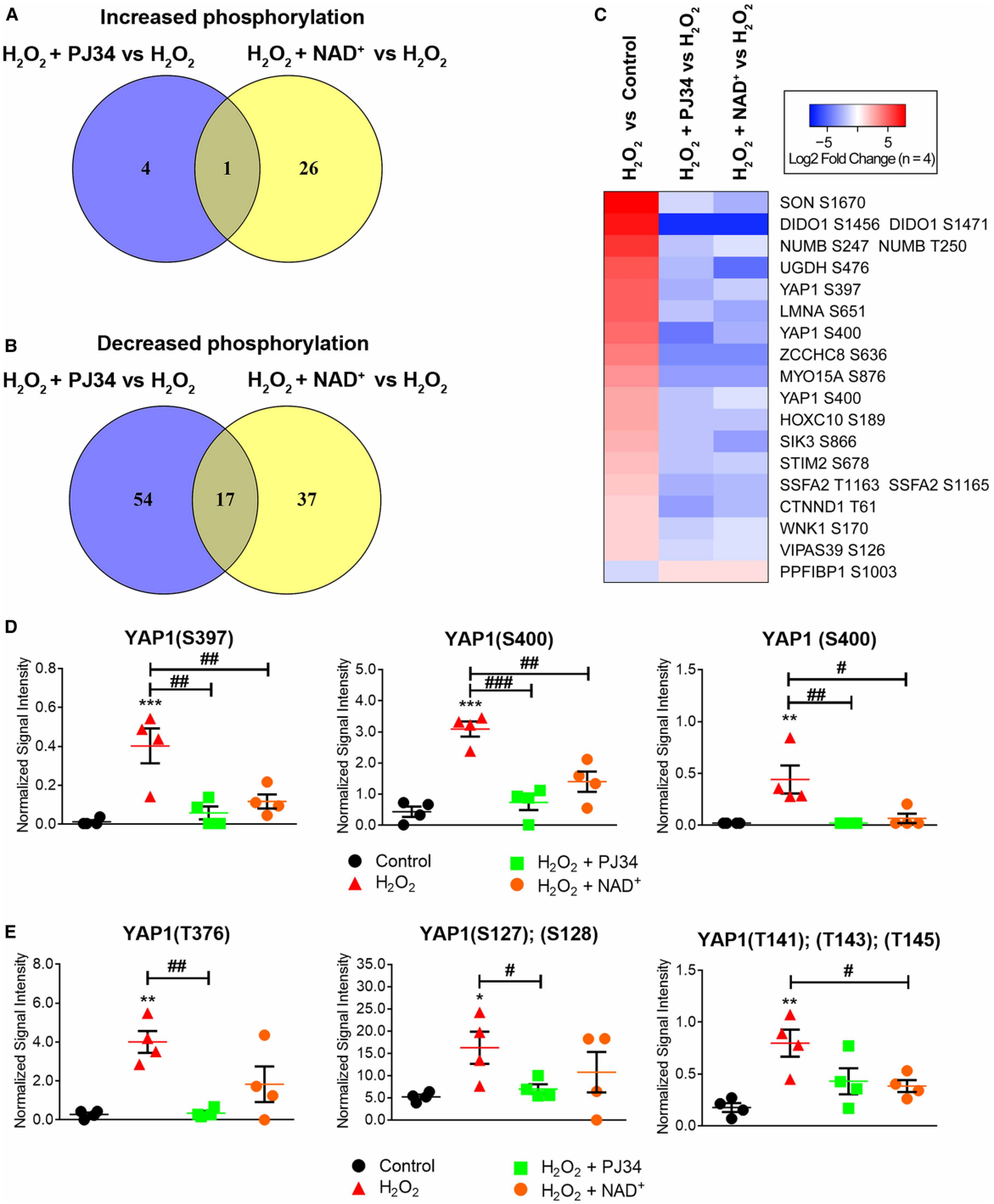

Figure 3. PARP-1 inhibitor PJ34 and NAD$^+$ supplementation reduced the phosphorylation induced by H_2O_2 treatment of YAP1 and other proteins. Part 1 of 2

(**A**) Venn diagram showing the number of phosphopeptides in which PJ34 inhibitor or NAD$^+$ supplementation increased significantly the phosphorylation of peptides ($P \leq 0.05$, Log2 Fold Change ≥ 1) relative to cells treated only with H_2O_2 (H_2O_2 + PJ34 vs H_2O_2 and H_2O_2 + NAD$^+$ vs H_2O_2, respectively). (**B**) Venn diagram showing the number of phosphopeptides in which PJ34 inhibitor or NAD$^+$ supplementation decreased significantly the phosphorylation of peptides ($P \leq 0.05$, Log2 Fold Change ≤ -1) relative to cells treated only with H_2O_2 (H_2O_2 + PJ34 vs H_2O_2 and H_2O_2 + NAD$^+$ vs H_2O_2, respectively). For Venn diagrams, only phosphopeptides that were significantly increased or decreased after H_2O_2 treatment were considered (H_2O_2 vs Control presented $P \leq 0.05$ and Log2 Fold Change ≤ -1 or ≥ 1). (**C**) Heatmap showing common phosphopeptides between

Biochemical Journal (2020) **477** 4491–4513
https://doi.org/10.1042/BCJ20200525

Figure 3. PARP-1 inhibitor PJ34 and NAD$^+$ supplementation reduced the phosphorylation induced by H_2O_2 treatment of YAP1 and other proteins. Part 2 of 2

H_2O_2 + PJ34 and H_2O_2 + NAD$^+$ obtained from Venn diagrams in (**A**) and (**B**). Red and blue colours indicates higher (Log2 Fold Change ≥ 1) and lower (Log2 Fold Change ≤ −1) phosphorylation in the studied comparison. **(D)** Normalized signal intensity obtained from LC–MS/MS analysis showing the common phosphopeptides (included in (**C**)) identified for YAP1. (**E**) Normalized signal intensity obtained from LC–MS/MS analysis showing other phosphopeptides identified for YAP1 protein not included in (**C**). In dot plots, the *y*-axis represents the normalized signal intensity obtained by LC–MS/MS analysis for each treatment. Data points represent individual independent observations ($n = 4$) collected on different days and processed separately. Mean and ± SEM are also represented. $^{***}P \leq 0.001$, $^{**}P \leq 0.01$ and $^{*}P \leq 0.05$ relative to control cells (H_2O_2 non-treated cells); $^{\#\#\#}P \leq 0.001$, $^{\#\#}P \leq 0.01$ and $^{\#}P \leq 0.05$ relative to H_2O_2 treatment.

PARP-1 silencing mitigated the reduction in cell viability induced by H_2O_2 and modified the phosphorylation pattern in WRL68 cells

The results showed above suggest that H_2O_2-induced PARP-1 activation promoted the phosphorylation of various proteins, including the transcriptional co-activator YAP1. To specifically abolish the activity of PARP-1, WRL68 cells were transfected with siRNA targeting human PARP-1 (siPARP-1). Once confirmed that siPARP-1 transfection effectively reduced PARP-1 expression compared with cells transfected with non-targeting siRNA (siNT) (Figure 4A), WRL68 cells were treated with H_2O_2, and were subjected to viability and phosphoproteomics analysis as indicated in Figure 4B. Silencing of PARP-1 resulted in an increase in cell viability 24 h after the oxidative treatment with H_2O_2, which confirmed the protective effect of blocking PARP-1 activity in WRL68 cells subjected to oxidative damage (Figure 4C).

Phosphoproteome analysis of siNT-transfected cells showed that treatment with H_2O_2 significantly modified the phosphorylation of multiple peptides (Figure 5A and Supplementary Dataset S1). To analyze the effect of blocking PARP-1 with siRNA after oxidative stress, we selected the phosphopeptides significantly increased after H_2O_2 treatment in siNT cells and analyzed the effect of silencing PARP-1 under oxidative stress conditions (siPARP-1 + H_2O_2 vs siNT + H_2O_2). Similar to pharmacological inhibition of PARP-1 or NAD$^+$ supplementation, PARP-1 silencing decreased the phosphorylation of peptides significantly phosphorylated after H_2O_2 treatment, including the phosphorylation of YAP1 at Thr376 (Figure 5B) suggesting that the phosphorylation of these peptides was dependent on PARP-1 activity.

GO analysis (using phosphopeptides differentially regulated after H_2O_2 treatment in cells with active and silenced PARP-1) showed that, after oxidative treatment, cells with active PARP-1 (siNT) modified the phosphorylation of proteins linked to multiple terms but none of the 10 most represented terms (significant terms with the largest number of genes) was involved in transcription (Figure 5C). However, cells with silenced PARP-1 (siPARP-1) modified the phosphorylation of proteins linked to a transcription-related term after oxidative treatment (Figure 5D, diagonal stripe bars). Interestingly, taking together the GO shown in Figure 2B,C and 5D, the GO term '*positive regulation of transcription from RNA polymerase II promoter*' was always presented and displayed a high number of genes when oxidative treatment was combined with PJ34 inhibitor or NAD$^+$ supplementation or PARP-1 was silenced, which suggested a role of PARP-1 activity in the transcription process under oxidative stress.

Therefore, PARP-1 silencing was relevant for the phosphoproteome and survival of cells exposed to the oxidative treatment, producing similar effects to PARP-1 inhibition and NAD$^+$ supplementation.

PARP-1 silencing reduced the phosphorylation of YAP1 in WRL68 cells after the oxidative treatment

For a more detailed study, we selected and compared proteins with phosphopeptides significantly increased after H_2O_2 treatment and significantly modified after PARP-1 silencing or treatment with PJ34 inhibitor or NAD$^+$ in the presence of H_2O_2 (Figure 6). There were no common proteins (i.e. containing phosphopeptides modified across the three comparisons done) which showed an increased phosphorylation (Figure 6A). However, 'UDP-glucose 6-dehydrogenase' (UGDH), 'stromal interaction molecule 2' (STIM2), and YAP1, protein previously mentioned (see Figure 3D) presented a decreased phosphorylation in all three comparisons (Figure 6B). Interestingly, those proteins have been related with stress response or their activity depend on NAD$^+$ [27,39,40]. Since H_2O_2-induced phosphorylation of YAP1 is reduced by pharmacological and genetic

Biochemical Journal (2020) **477** 4491–4513
https://doi.org/10.1042/BCJ20200525

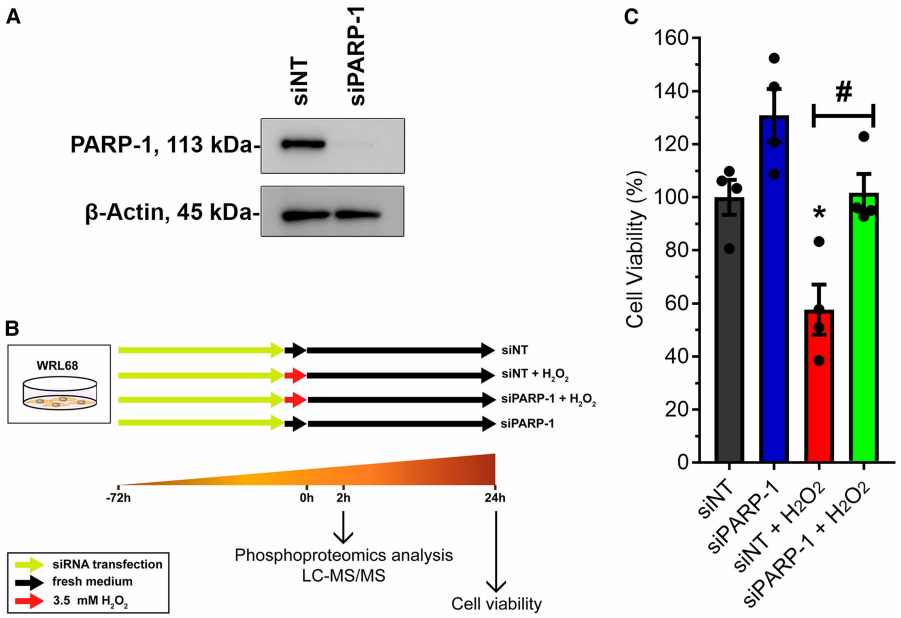

Figure 4. Silencing of PARP-1 increased the viability of WRL68 cells subjected to H_2O_2 treatment.

(**A**) Representative Western Blot showing the efficiency of silencing PARP-1 by siRNA in WRL68 cells. β-actin was used as loading control. (**B**) Experimental workflow for PARP-1 silencing and treatment in WRL68 cells. After siRNA transfection, WRL68 cells were exposed to a single dose of H_2O_2 for 30 min (3.5 mM). Upon oxidative treatment, cells were further incubated in fresh medium (without H_2O_2) for 2 h to perform phosphoproteomics analysis or for 24 h to measure cell viability. As negative control of transfection, WRL68 cells transfected with siRNA non-target (siNT) were used. (**C**) Viability of WRL68 cells analyzed with MTS assay after 24 h of exposure to H_2O_2. Cell viability was expressed as percentage of viable cells respect to siNT-control cells (H_2O_2 non-treated cells), which was considered 100%. Black dots represent individual independent observations ($n = 4$), and bar plots indicate mean ± SEM. $^{*}P \leq 0.05$ relative to control cells (H_2O_2 non-treated cells); $^{\#}P \leq 0.05$ relative to H_2O_2 treatment.

inactivation of PARP-1 and by NAD^+ supplementation and YAP1 activity is related with response to oxidative stress, cell growth, proliferation and survival [27,41], we decided to study more in detail the link between PARP-1 activity and YAP1 phosphorylation. Initially, we analyzed the effect of PARP-1 activity on YAP1 phosphorylation. Similar to PJ34 inhibitor or NAD^+ supplementation, PARP-1 silencing also reduced the H_2O_2-induced phosphorylation of YAP1 at Thr376 and Ser400 (Figure 6C). Moreover, it showed the same trend for the peptides carrying the phosphorylation at Ser400 and Ser403 (Figure 6C). All together, these results showed that H_2O_2-induced PARP-1 activation promoted YAP1 phosphorylation.

YAP1 promoted the viability of WRL68 cells after oxidative treatment

YAP1 phosphorylation at Ser127, Ser400 and Ser403 is related with its cytoplasmic retention and degradation, which in turn results in a decreased expression of genes related with cell survival [21–23,42]. Thus, our results on YAP1 phosphorylation (Figures 3D,E and 6C), suggested that H_2O_2-induced PARP-1 activation could regulate YAP1 stability. To validate our hypothesis, we treated WRL68 cells as indicated in Figure 1A and examined the protein levels at different time points after H_2O_2 treatment. Interestingly, YAP1 showed a decrease in its protein levels 4 and 6 h after the oxidative treatment (Figure 7A). Inhibition of PARP-1 activity with PJ34 counteracted the decrease in YAP1 protein levels 6 h after H_2O_2 treatment (Figure 7B,C). These results suggested that the phosphorylations observed in YAP1 were related with its stability and degradation.

YAP1 participates in the response to stress and proliferation [27,41] and PARP-1 activity after oxidative treatment regulated YAP1 phosphorylation and stability. Thus, we used siRNA techniques to analyze whether the PARP-1 dependent regulation of YAP1 played a role in the survival of WRL68 cells subjected to oxidative treatment (Figure 8A). As expected, the silencing of PARP-1 was able to increase the cell viability of WRL68 cells treated with H_2O_2 (Figure 8B, green bar). Interestingly, the silencing of YAP1 (siYAP1) in WRL68 cells

Biochemical Journal (2020) 477 4491–4513
https://doi.org/10.1042/BCJ20200525

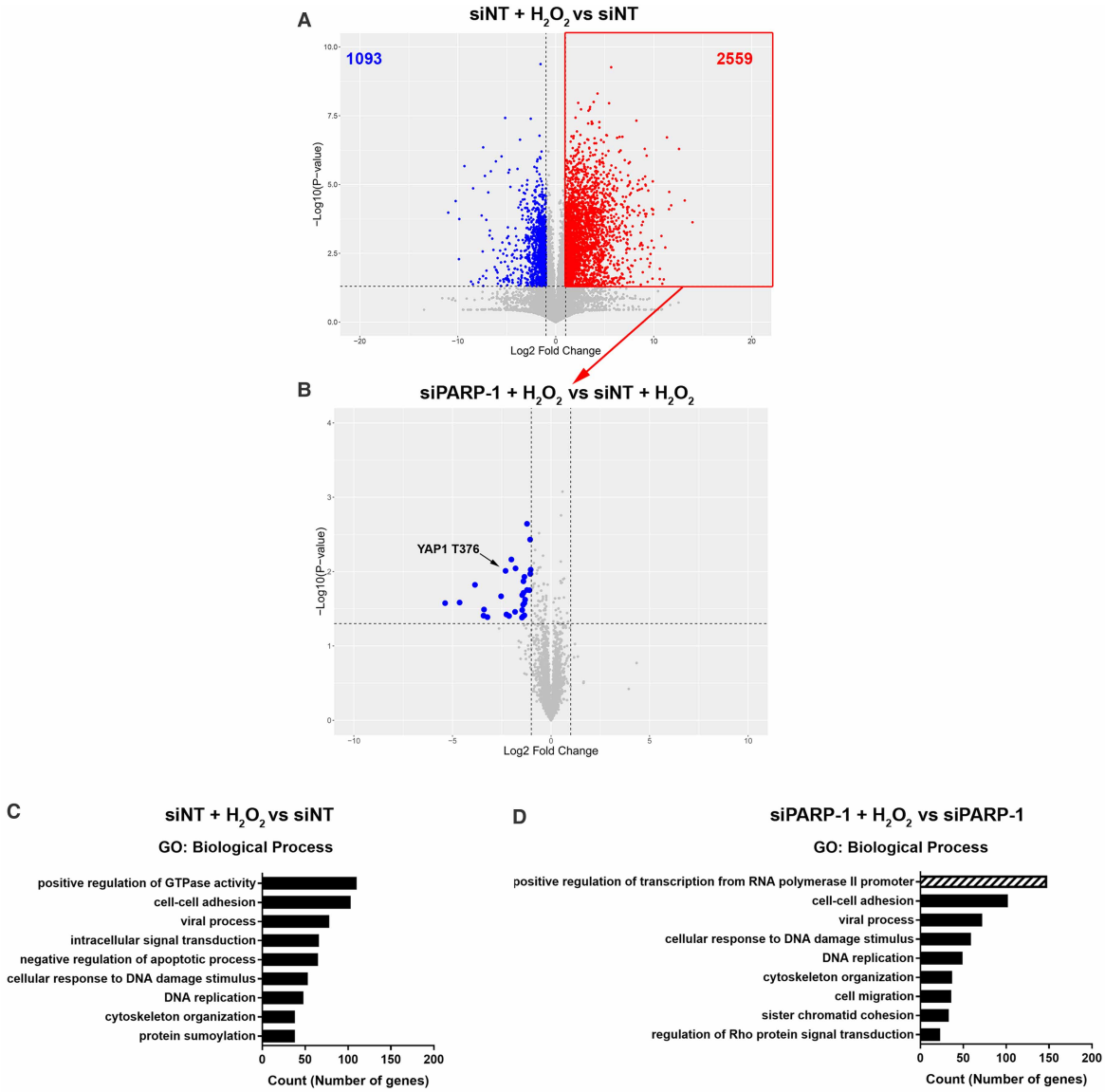

Figure 5. PARP-1 silencing reduced the H_2O_2-induced phosphorylation of multiple proteins and increased the number of proteins with modified phosphorylation that are linked to transcription in WRL68 cells.

(**A**) Volcano plot showing the phosphopeptides identified by LC–MS/MS analysis after oxidative treatment in siNT-transfected WRL68 cells. The *x*-axis represents the degree of phosphorylation (Log2 Fold Change) respect to siNT-control cells (H_2O_2 non-treated cells), and the *y*-axis shows their statistical significance (–Log10 *P*-value). Horizontal and vertical dashed lines indicate the filtering criteria (*P*-value = 0.05 and Log2 Fold Change = ± 1.0, respectively). Red and blue dots correspond to phosphopeptides that changed significantly in experimental conditions respect to control cells ($P \leq 0.05$, Log2 Fold Change ≥ 1 and Log2 Fold Change ≤ -1, respectively), while grey dots represent phosphopeptides that did not match with the filtering criteria ($P \geq 0.05$, Log2 Fold Change > -1 or Log2 Fold Change < 1). Blue and red numbers represent the number of phosphopeptides with significant decreased (Log2 Fold Change ≤ -1, $P \leq 0.05$) and increased (Log2 Fold Change ≥ 1, $P \leq 0.05$) phosphorylation, respectively. (**B**) Volcano plot that shows the effect of silencing PARP-1 in phosphopeptides with increased phosphorylation in siNT + H_2O_2 cells (red dots in (**A**)). The *x*-axis represents the Log2 Fold Change in the comparison siPARP-1 + H_2O_2 versus siNT + H_2O_2. (**C** ,**D**) DAVID Bioinformatics analyses to determine GO enrichment for Biological Process terms from significant modified phosphopeptides in H_2O_2-treated cells in the negative control of transfection (siNT, (**C**)) and in cells with PARP-1 silenced (siPARP-1, (**D**)). Each bar graph represents the number of genes corresponding to each term; only the 10 most populated terms (significant terms associated with more genes) are represented. The bar chart with diagonal stripes highlights the GO terms related with transcription processes.

Biochemical Journal (2020) **477** 4491–4513
https://doi.org/10.1042/BCJ20200525

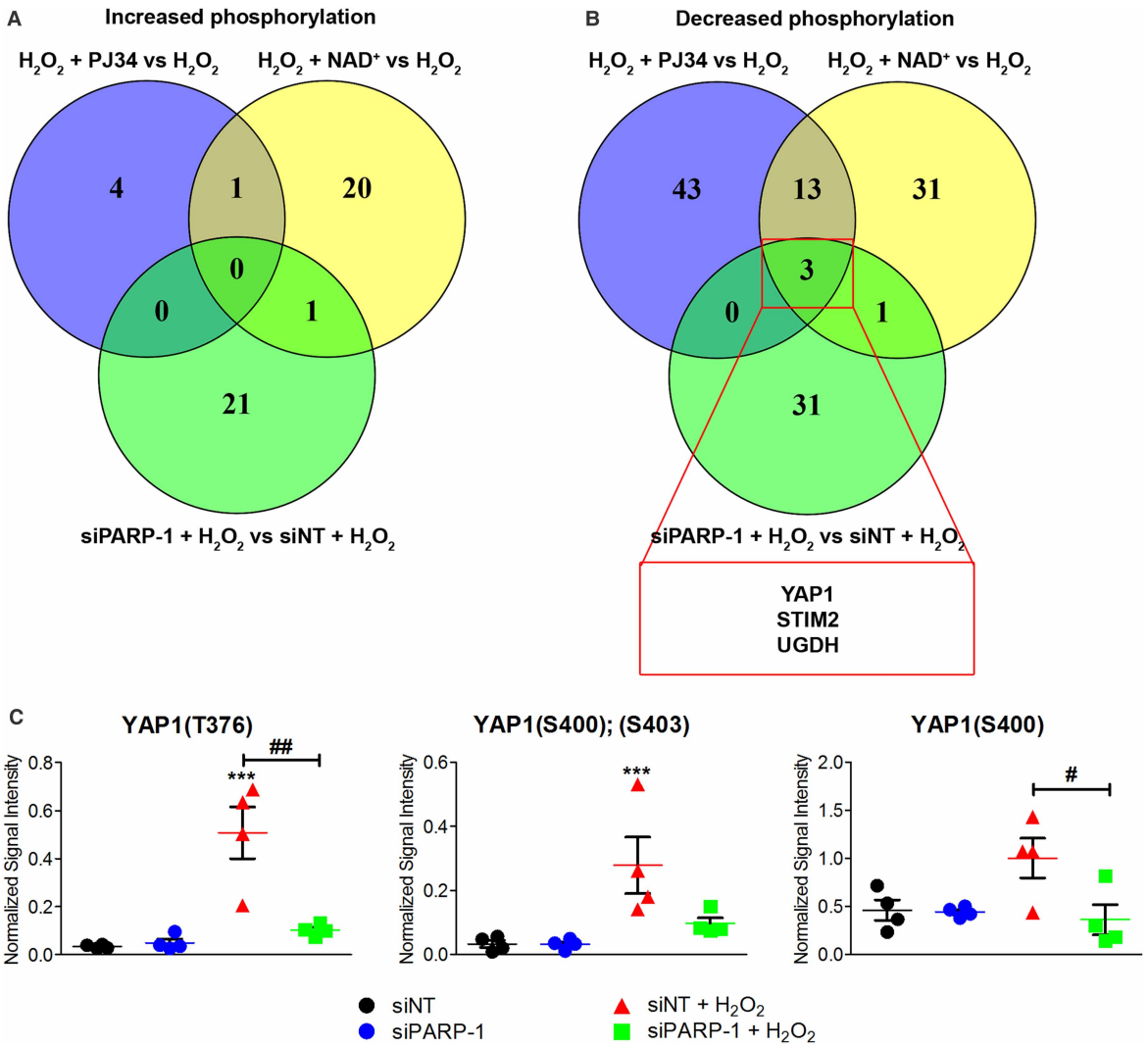

Figure 6. Reduction of PARP-1 activity using PJ34 inhibitor or siRNA, and NAD$^+$ supplementation reduced YAP1 phosphorylation induced by H_2O_2.

(**A**) Venn diagram showing the number of proteins in which PJ34 inhibitor, PARP-1 silencing or NAD$^+$ supplementation increased significantly their phosphorylation ($P \leq 0.05$, Log2 Fold Change ≥ 1) respect to cells treated with H_2O_2 (H_2O_2 + PJ34 vs H_2O_2, H_2O_2 + NAD$^+$ vs H_2O_2 and siPARP-1 + H_2O_2 vs siNT + H_2O_2, respectively). (**B**) Venn diagram showing the number of proteins in which PJ34 inhibitor, PARP-1 silencing or NAD$^+$ supplementation decreased significantly their phosphorylation ($P \leq 0.05$, Log2 Fold Change ≤ -1) respect to cells treated with H_2O_2 (H_2O_2 + PJ34 vs H_2O_2, H_2O_2 + NAD$^+$ vs H_2O_2 and siPARP-1 + H_2O_2 vs siNT + H_2O_2, respectively). The three common proteins identified in the treatments (YAP1, STIM2 and UGDH) are indicated. For Venn diagrams, only proteins with a significantly modified phosphorylation in H_2O_2-treated cells were considered (H_2O_2 vs control for PJ34 and NAD$^+$ treatments or siNT + H_2O_2 vs siNT for siPARP-1 silencing, $P \leq 0.05$ and Log2 Fold Change ≤ -1 or ≥ 1). (**C**) Normalized signal intensity obtained from LC–MS/MS analysis showing YAP1 phosphopeptides identified in siRNA assays. The *y*-axis represents the normalized signal intensity obtained by LC–MS/MS analysis for each treatment. Data points represent individual independent observations ($n = 4$) collected on different days and processed separately. Mean and ± SEM are also represented. $^{***}P \leq 0.001$ relative to control cells (H_2O_2 non-treated cells); $^{\#\#}P \leq 0.01$ and $^{\#}P \leq 0.05$ relative to H_2O_2 treatment.

Biochemical Journal (2020) **477** 4491–4513
https://doi.org/10.1042/BCJ20200525

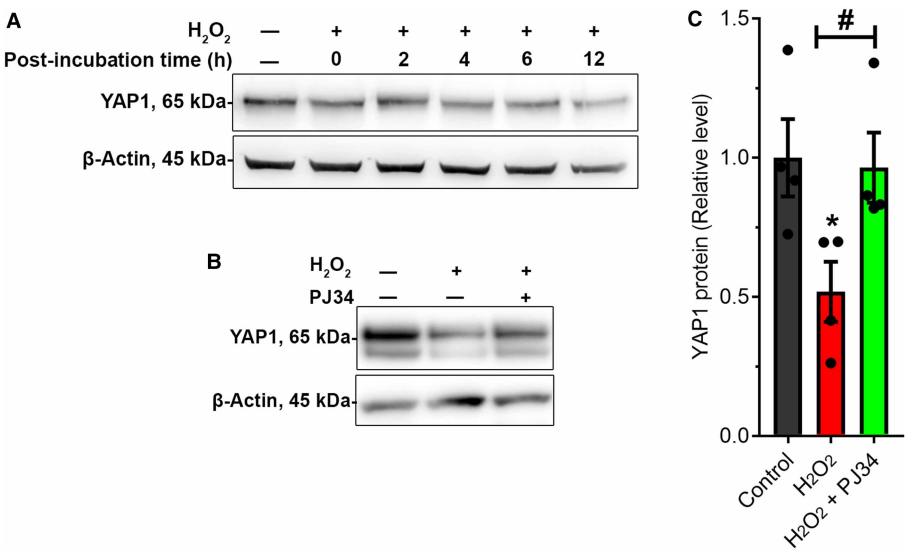

Figure 7. PARP-1 inhibition increased YAP1 protein levels in WRL68 cells treated with H_2O_2.

(**A**) Representative Western Blot showing YAP1 protein levels in control cells and H_2O_2-treated cells post-incubated for 0, 2, 4, 6 and 12 h. β-Actin was used as loading control. (**B**) Representative Western Blot showing YAP1 protein levels in control cells and H_2O_2-treated cells post-incubated for 6 h in absence or presence of PJ34 inhibitor. β-actin was used as loading control. (**C**) Densitometry analysis of YAP1 protein levels normalized to the levels of the loading control β-actin and expressed as relative to control cells in the conditions described in (**B**). Black dots represent individual independent observations ($n = 4$) collected on different days and processed separately, and bar plots indicate mean ± SEM. $^{*}P \leq 0.05$ relative to control cells (H_2O_2 non-treated cells); $^{\#}P \leq 0.05$ relative to H_2O_2 treatment.

subjected to H_2O_2 treatment abolished the protective effect of blocking PARP-1 activity, since the silencing of PARP-1 was not able to increase the cell viability of WRL68 cells treated with H_2O_2 when YAP1 was also silenced (Figure 8B, yellow bar). In line with our data showing that PARP-1 activity induced the degradation of YAP-1, siYAP1 when PARP-1 was active did not show any significant recovery (Figure 8B, purple bar). These results also indicated that YAP1 was relevant for the survival of WRL68 cells subjected to H_2O_2 treatment, since the siYAP1 in H_2O_2 non-treated cells did not show any significant effect (Figure 8B). In summary, PARP-1-dependent regulation of YAP1 played a role in the survival of WRL68 cells subjected to oxidative treatment.

Differential kinase activities upon PARP-1 silencing in H_2O_2-treated cells

Our data demonstrated that the reduction in PARP-1 activity in cells suffering oxidative stress reduced the phosphorylation and degradation of YAP1 (Figures 3D,E, 6C, 7B,C). Since the phosphorylation of YAP1 is considered as the main factor regulating its activity [26], we investigated the mechanism that PARP-1 could use to promote YAP1 phosphorylation. Thus, we determine the protein-kinases implicated in the changes of protein phosphorylation observed after the oxidative treatment, using KSEA, an algorithm that estimates kinase activities according to the phosphorylation status of their substrates [36]. KSEA analysis showed that H_2O_2 treatment of siNT cells significantly ($P \leq 0.05$) modified the activity of multiple kinases (Figure 9A); increasing the activity of SRC, MAPK14, AKT1, AMPK and PRKACA; and decreasing the activity of other kinases, such as GSK3A, GSK3B, CDK1, MTOR and CDK2 (Figure 9A). Of notice, cells with a silenced expression of PARP-1, the effect of H_2O_2 on AMPK (AMP-activated protein kinase) and mTOR (mammalian target of rapamycin) activities was not significant, and it was of a lower magnitude when compared with the effect of H_2O_2 on siNT cells (Figure 9A). To corroborate the changes in AMPK and mTOR activities, we analyzed the phosphorylation level of all the identified substrates by KSEA in our data set (Figure 9B). As expected, the silencing of PARP-1 remarkably reduced the overall phosphorylation of AMPK substrates after H_2O_2 treatment (siPARP-1 + H_2O_2; mean of the fold change values = 0.27 ± 0.21) compared with siNT-transfected cells treated with H_2O_2 (siNT + H_2O_2; mean of the fold change values = 0.62 ± 0.28) (Figure 9B). In addition, we determined that classical

Biochemical Journal (2020) **477** 4491–4513
https://doi.org/10.1042/BCJ20200525

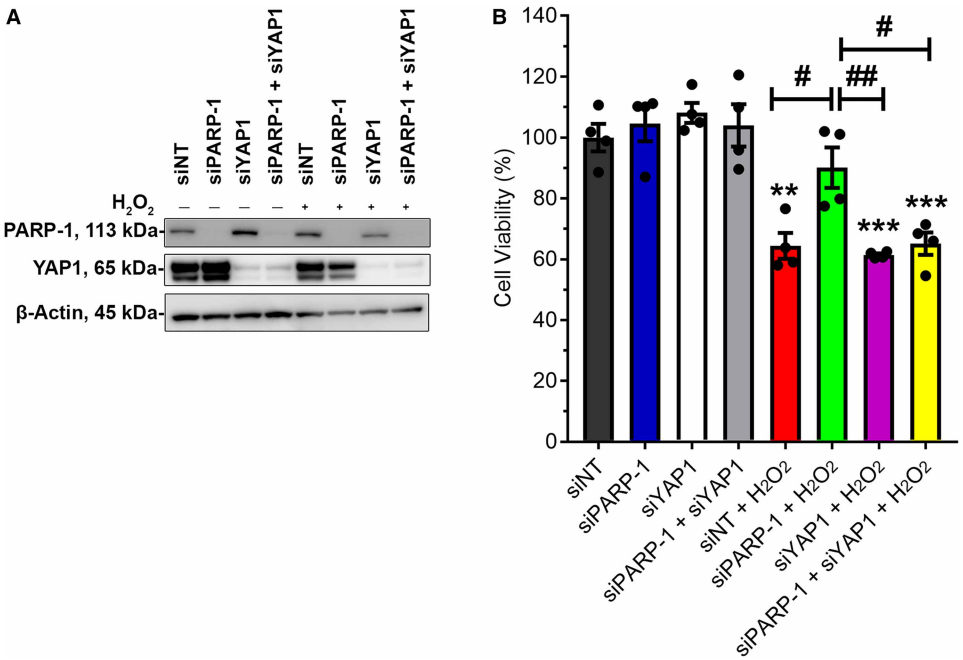

Figure 8. YAP1 silencing abrogated the protective effect of silencing PARP-1 on WRL68 cells subjected to H_2O_2 treatment.

(**A**) Representative Western Blot showing the protein levels of PARP-1 and YAP1 after siRNA silencing of PARP-1 and/or YAP1 in WRL68 cells. β-actin was used as loading control. (**B**) Viability of WRL68 cells analyzed with MTS assay 24 h after H_2O_2 treatment in transfected cells. Cell viability was expressed as percentage of viable cells respect to siNT-control cells (H_2O_2 non-treated cells), which was considered 100%. Black dots represent individual independent observations ($n = 4$) collected on different days and processed separately, and bar plots indicate mean ± SEM. $^{**}P \leq 0.01$ and $^{***}P \leq 0.001$ relative to siNT-control cells (H_2O_2 non-treated cells); $^{\#}P \leq 0.05$ and $^{\#\#}P \leq 0.01$ relative to H_2O_2 treatment.

substrates of AMPK, such as acetyl-CoA carboxylase 1 (ACC1) and TBC1D1 [43,44], showed decreased phosphorylation when PARP-1 was silenced in H_2O_2-treated cells (Figure 9C).

Contrary to AMPK substrates, the phosphorylation of mTOR substrates did not show any relevant different between siNT and siPARP-1 cells after the oxidative treatment (mean of fold change values for siNT + H_2O_2 = -0.39 ± 0.16, and for siPARP-1 + H_2O_2 = −0.42 ± 0.23) (Figure 9D). In agreement with that, the substrates of mTOR 'Eukaryotic translation initiation factor 4E-binding protein 1' (EIF4EBP1) and 'La-related protein 1' (LARP1) [45,46] showed only a slight increase in phosphorylation in siPARP-1 cells treated with H_2O_2 respect to siNT cells (Figure 9E). These results suggested that PARP-1 activation had a stronger effect on AMPK activity than in mTOR.

We previously showed that NAD^+ supplementation also reduced the phosphorylation of various proteins including YAP1 (Figure 3D,E), suggesting that NAD^+ depletion induced by PARP-1 activation may be responsible for the changes observed in the phosphoproteome of WRL68 cells subjected to oxidative stress. As AMPK is one of the major energy sensors in cells, and PARP-1 activation promotes NAD^+ depletion and subsequently ATP depletion [8,30,47,48]; we studied the changes in AMPK activity under NAD^+ supplementation in WRL68 cells subjected to H_2O_2 treatment. Interestingly, NAD^+ supplementation and the presence of PJ34 inhibitor decreased the phosphorylation of the AMPK substrate TBC1D1 in cells treated with H_2O_2 (Figure 9F). This evidence suggested that the alteration of NAD^+ levels caused by PARP-1 activation may be responsible for the changes in the activity of kinases, including AMPK, and consequently responsible for the phosphorylation of the downstream targets for these kinases.

Discussion

In the present study, we characterized the impact of PARP-1 activity on the phosphoproteome of WRL68 cells after oxidative damage. Phosphoproteomics analysis showed that H_2O_2 significantly changed the

Biochemical Journal (2020) **477** 4491–4513
https://doi.org/10.1042/BCJ20200525

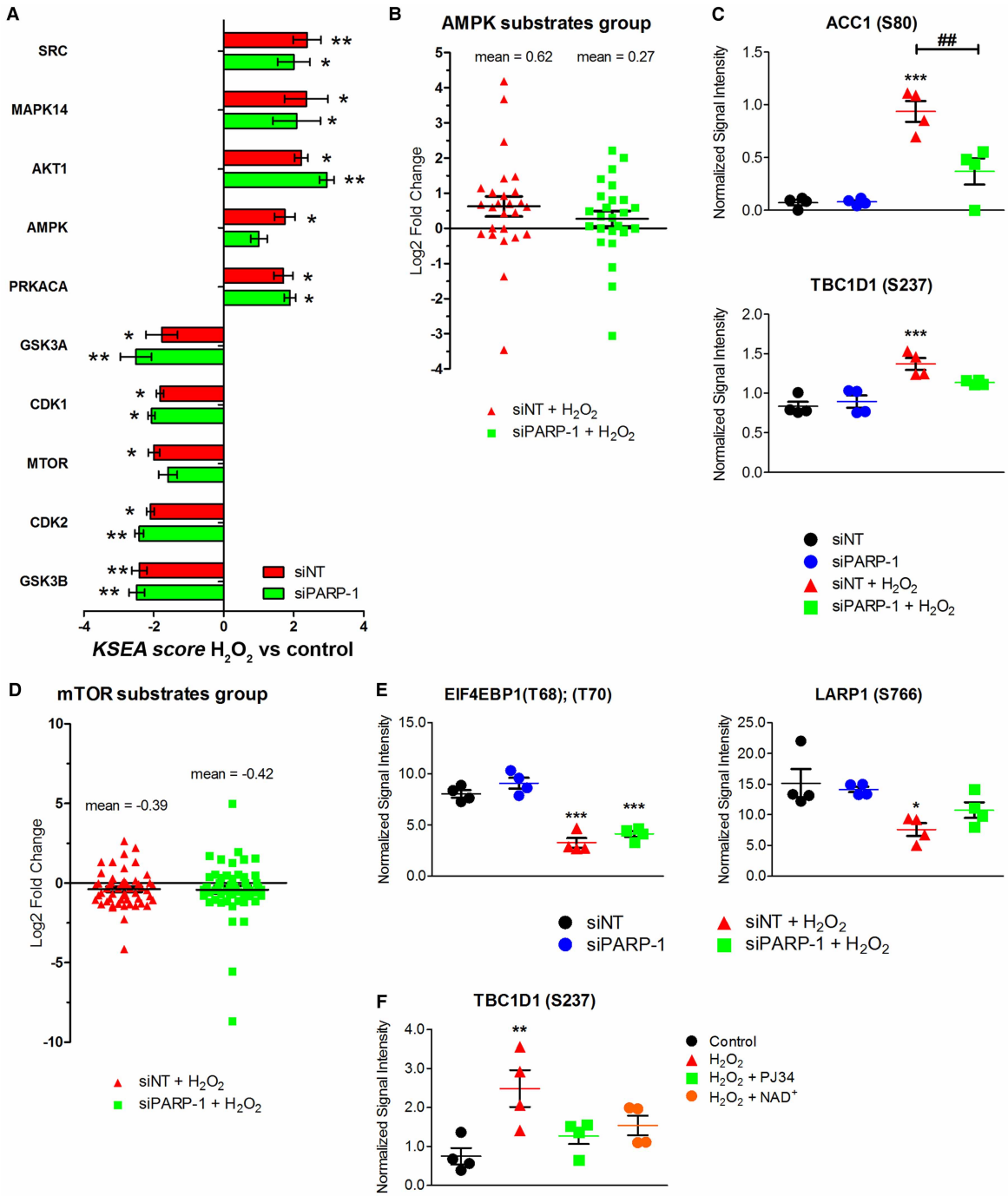

Figure 9. Silencing of PARP-1 reduced AMPK activation in WRL68 cells subjected to H_2O_2 treatment. Part 1 of 2

(**A**) Kinase-substrate enrichment analysis (KSEA) was performed using phosphoproteomics data from siRNA experiments. Bars represent the KSEA scores obtained for each kinase after H_2O_2 treatment compared with H_2O_2 non-treated (control) cells in siNT and siPARP-1 cells. Only the kinases in which KSEA scores were obtained using five or more substrates were considered. Positive and negative KSEA scores indicate activation and inhibition of kinases, respectively. *Z*-test was used to evaluate the statistical significance of comparing H_2O_2 respect to H_2O_2 non-treated in siNT- and siPARP-1-transfected cells. $^{*}P \leq 0.05$ and $^{**}P \leq 0.01$. (**B**) All the substrates for the kinase AMPK identified in KSEA analysis were represented indicating its phosphorylation degree (Log2 Fold Change) respect to H_2O_2 non-treated in siNT- and siPARP-1-transfected cells. The average phosphorylation of each group is indicated. (**C**) Normalized signal intensity obtained from LC–MS/MS analysis showing the phosphorylation of AMPK substrates, ACC1 and TBC1D1 at Ser80 (S80) and Ser237 (S237), respectively. (**D**) All the substrates

Figure 9. Silencing of PARP-1 reduced AMPK activation in WRL68 cells subjected to H_2O_2 treatment. Part 2 of 2

for the kinase mTOR identified in KSEA analysis were represented indicating its phosphorylation degree (Log2 Fold Change) respect to H_2O_2 non-treated in siNT- and siPARP-1-transfected cells. The average phosphorylation of the group is indicated. (**E**) Normalized signal intensity obtained from LC–MS/MS analysis showing the phosphorylation of mTOR substrates, EIF4EBP1 and LARP1. (**F**) Normalized signal intensity obtained from LC–MS/MS analysis showing the phosphorylation of TBC1D1 at Ser237 (S237) using PJ34 inhibitor or NAD^+ supplementation. For (**C**), (**E**) and (**F**), the *y*-axis represents the normalized signal intensity obtained by LC–MS/MS analysis for each treatment. Data points represent individual independent observations ($n = 4$) collected on different days and processed separately. Mean and ± SEM are also represented. $^{***}P \leq 0.001$, $^{**}P \leq 0.01$and $^{*}P \leq 0.05$ relative to H_2O_2 non-treated cells; $^{\#\#}P \leq 0.01$ relative to H_2O_2 treatment.

phosphorylation pattern of WRL68 cells (Figure 2A). The pharmacological or genetic reduction in PARP-1 activity prevented part of the phosphoproteome alterations induced by ROS (Figures 3A–C and 5B) indicating that some of these alterations were dependent on PARP-1 activity. Other studies have also shown that PARP-1 promoted the activation of kinases and cell death [49,50].

It has been described that PARP-1 participates in the regulation of transcription [51-53], and here we have shown that the reduction in PARP-1 activity under oxidative damage increased the number of proteins related to the transcription processes that increase or decrease their phosphorylation (Figures 2B and 5D). In particular, PARP-1 activation induced by oxidative damage increased the phosphorylation of the transcriptional co-activator YAP1 (Figures 3C–E, 6B,C), the final effector of the Hippo pathway [54]. In the Hippo pathway, LATS1/2 phosphorylates YAP1 at Ser127/397 and promotes its cytoplasmic retention [21]. In addition, the phosphorylation YAP1 at Ser397 prompts the phosphorylation at Ser400/403 by the casein-kinase 1 (CK1ε/δ), which in turn promotes its degradation [22]. In our study, pharmacological and genetic inhibition of PARP-1 reduced the H_2O_2-induced phosphorylation of YAP1 at those residues (Figures 3D,E and 6C). Furthermore, PARP-1 inhibition prevented the reduction in YAP-1 protein levels induced by H_2O_2 (Figure 6). These results suggest that PARP-1 activation promotes YAP1 phosphorylation and degradation under oxidative damage.

YAP1 plays an important role in the response to oxidative stress and regulates the expression of antioxidant enzymes including catalase and MnSOD [27,55]. In fact, YAP1 depletion promotes H_2O_2-induced cell death, while its expression prevents them [56]. We showed that the reduction in PARP-1 activity under oxidative treatment protected YAP1 from degradation and increased cell viability (Figures 4C, 6B and 7C). PARP-1 silencing rescued cell viability under oxidative damage only when YAP1 was not silenced (Figure 8B); clearly indicating that YAP1 is necessary for the protective role of the reduction in PARP-1 activity after oxidative damage. Furthermore, our results showed that the depletion of YAP1 did not affect the viability of cells not subjected to H_2O_2 treatment (Figure 8B), suggesting that, in WRL68 cells, YAP1 activity is relevant for cell viability only when oxidative damage is present. These results are in agreement with the fact that YAP1 is important for the recovery after a harmful situation [56-63]. Therefore, YAP1 degradation promoted by PARP-1 activation may alter the capacity of WRL68 cells to respond to oxidative damage, leading to cell death. Further studies are needed to characterize the molecular mechanism downstream of YAP1 that promotes the survival of WRL68 after oxidative stress.

PARP-1 plays a relevant role in the repair of DNA damage and long-term inhibition of PARP-1 could increase DNA damage [64]. However, long-term inhibition PARP-1 after oxidative stress exposure still presented a protective effect (Supplementary Figure S1). Thus, the potential increase in DNA damage after long-term inhibition of PARP-1 did not reverse the protective effect of blocking PARP-1 in WRL68 cells. In addition, 4 h after oxidative stress exposure, PARP-1 inhibition reduced the DNA damage induced by H_2O_2 in our WRL68 model (Supplementary Figure S2). The reduction in DNA damage could be linked to the improvement of mitochondrial activity and redox homeostasis that PARP-1 inhibition during oxidative stress produces in this cell model [30]. Further studies are needed to determine if YAP1 plays any role in the improvement of the mitochondrial function or the reduction in unrepaired DNA damage observed after PARP-1 inhibition during oxidative stress.

Under certain circumstances (i.e. excessive DNA damage), PARP-1 activation depletes NAD^+ which promotes a drop of ATP levels and induces cell death [8,10,11,30,65]; but NAD^+ supplementation prevents those effects [30,48,66,67]. Similar to the reduction in PARP-1 activity, the supplementation with NAD^+ during oxidative treatment modified the phosphorylation of multiple proteins linked to transcription processes (Figure 2C) and prevented part of the phosphorylations induced by the oxidative treatment (Figure 3A,B). Furthermore, the addition of NAD^+ reduced the phosphorylation of YAP1 at Ser397 and Ser400 and produced

Biochemical Journal (2020) 477 4491–4513
https://doi.org/10.1042/BCJ20200525

a similar trend at other YAP1 sites, including Ser127 (Figure 3D,E). These results suggested that some changes observed in the phosphoproteome including the phosphorylation of YAP1 are related with a decrease in the levels of NAD^+ after PARP-1 activation under oxidative damage.

NAD^+ levels are mainly controlled by the savage pathway in mammalian cells and nicotinamide phosphoribosyltransferase (NAMPT) is a key regulator of the salvage pathway [68]. In aged animals, decreased expression of NAMPT reduces NAD^+ levels, affecting the activities of NAD^+-dependent enzymes and supplementation with NAD^+ intermediates, such as nicotinamide mononucleotide (NMN) and nicotinamide riboside (NR), can effectively restore the NAD^+ pool and multiple cellular functions [69-71]. Conversely, NAMPT overexpression in multiple cancer cells favours cell proliferation and survival and NAMPT inhibitors like FK866 are been tested as potential therapeutic drugs [72].

Our data indicate that PARP-1 inhibition under oxidative stress conditions prevented the depletion of NAD^+ that increased the phosphorylation and degradation of YAP1. However, a long-term inhibition of PARP-1 could increase the DNA damage and reduce the cell viability. As an alternative, we found that direct administration of NAD^+ reduced YAP1 phosphorylation under oxidative stress conditions. Thus, future work will establish whether supplementation with the NAD^+ precursors NMN or NR preserve the stability and protective functions of YAP1 without compromising the beneficial role of PARP-1 on DNA repair. Our data suggest that depletion of NAD^+ levels using NAMPT inhibitors like FK866 should increase YAP1 phosphorylation in cells with blocked PARP-1 activity exposed to oxidative stress. Future experiment assessing this hypothesis could further define whether the effects observed on YAP1 phosphorylation after PARP-1 inhibition are strictly via NAD^+ depletion or the actual activity or PARP-1 plays any role.

The drop in NAD^+ levels, and therefore in ATP levels, can generate a situation of energy stress and activate diverse signalling pathways to restore it, including the main energy sensor in cells, AMPK [47]. KSEA analysis showed an increase in AMPK activity after oxidative damage, and this activity was lower when PARP-1 was silenced (Figure 9A). H_2O_2 treatment significantly increased the phosphorylation of AMPK classical substrates ACC1 and TBC1D1 (Figure 9B,C). However, H_2O_2 was not able to significantly increase the phosphorylation of these substrates when PARP-1 was silenced (Figure 9B,C), which suggested that AMPK was activated because of PARP-1 activation. In agreement with our results, H_2O_2 treatment of Vascular Smooth Muscle Cells promotes PARP-1 and AMPK activation, while the inhibition of PARP-1 reduces the activation of AMPK [73]. Furthermore, ATP depletion caused by PARP-1 activation can promote the activation of AMPK and the inhibition of mTOR [4,74,75]. As mentioned before, the phosphorylation of AMPK substrate TBC1D1 at Ser237 was significantly increased after H_2O_2 treatment. However, H_2O_2 was not able to significantly increase the phosphorylation of TBC1D1 when the PARP-1 inhibitor PJ34 or NAD^+ were added (Figure 9F). All these evidences suggested that our oxidative treatment-induced PARP-1 activation and depleted NAD^+ levels which generated an energy stress in WRL68 cells, leading to AMPK activation.

In addition, the stability of YAP1 can also be modified by the energy status in the cell [76]. In fact, AMPK inhibits YAP1 activity by direct phosphorylation or by phosphorylation of the negative regulator of YAP1, AMOTL1 (Angiomotin Like protein 1) in response to an energy stress [76–78]. AMPK promotes YAP1 phosphorylation at Ser127, its cytoplasmic retention and inhibits the expression of YAP-target genes [77]. These evidences suggested that AMPK may be implicated in the phosphorylation of YAP1 in our system. However, further studies are needed to determine whether AMPK activation is involved directly or indirectly in YAP1 phosphorylation.

Taking together all the previously discussed data we propose a model (Figure 10). According to this model, PARP-1 activation after oxidative treatment depleted NAD^+ and ATP levels, and therefore, caused an energy stress that activated multiple kinases, including AMPK, that promoted changes in the phosphoproteome. Crucially, the drop in NAD^+ levels induced by PARP-1 activity, promoted the phosphorylation and the subsequent degradation of YAP1, a transcriptional co-activator relevant for the survival of WRL68 cells under oxidative stress. Genetic or pharmacological inhibition of PARP-1 or the restoration of NAD^+ levels reduced the energy stress, attenuated AMPK activity and mitigated some of the H_2O_2 effects over the phosphoproteome, including the decrease in the phosphorylation and degradation of the pro-survival transcriptional co-activator YAP1 (Figure 10).

Finally, the relationship between PARP-1 and YAP1 could be relevant in diseases related with high levels of oxidative stress. For example, in the non-alcoholic fatty liver disease (NAFLD) oxidative stress and PARP-1 activity are increased [79,80], and a recent phosphoproteomics analysis have shown that YAP1 phosphorylation increases as NAFLD worsens [81]. Thus, the potential role of the relationship between PARP-1 activation and

Biochemical Journal (2020) **477** 4491–4513
https://doi.org/10.1042/BCJ20200525

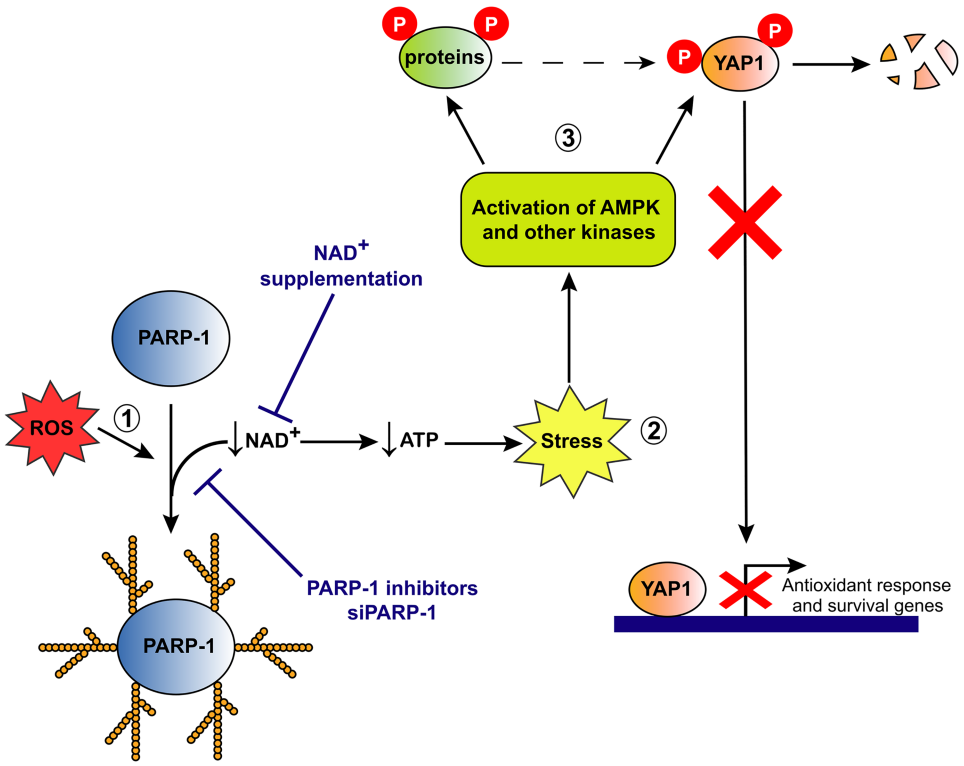

Figure 10. Proposed model of PARP-1 and YAP1 interaction under oxidative damage.

H_2O_2 treatment induced the activation of PARP-1 (**1**), which depletes NAD^+ levels, leading to a drop in ATP levels and a subsequent energy stress (**2**). The low levels of energy induced the activation of AMPK and other kinases, which modified the phosphorylation status of several proteins (**3**). The phosphorylation of the transcriptional co-activator YAP1 promoted its degradation, which reduced its activity as transcriptional co-activator and negatively affected the survival of WRL68 cells. The reduction in PARP-1 activity (by either pharmacological or siRNA strategies) or the restoration of NAD^+ levels, prevented the appearance of energy stress, the activation of AMPK and other kinases, and the subsequent YAP1 phosphorylation and degradation, which in turn increased the survival of WRL68 cells.

YAP1 phosphorylation in the diseases associated with high levels of oxidative stress should be addressed in future studies.

In summary, the present study shows that PARP-1 activation after oxidative damage induced the phosphorylation and degradation of YAP1, a transcriptional co-activator relevant for the survival of WRL68 cells under these conditions, suggesting a new potential target for the management of oxidative stress-induced cell death.

Data availability

The mass spectrometry proteomics data have been deposited to the ProteomeXchange Consortium via the PRIDE [82] partner repository with the dataset identifier PXD019823 and 10.6019/PXD019823. Sample details for each RAW file deposited in PRIDE can be found in Supplementary Dataset S1.

Competing Interests

The authors declare that there are no competing interests associated with the manuscript.

Funding

S.M.M.G. was funded by grants from Ministerio de Educación, Cultura y Deporte, Spain (FPU14/02219, EST16/00301 and EST17/00231). The work was funded by grant from Programa Operativo FEDER de Andalucía 2014-2020, Spain (B-CTS-185-UGR18). P.R.C., P.C., M.H. and V.R. were funded by grants from Barts and the London Charity (MIMG1M3R) and Cancer Research UK (C16420/A18066). The funding organizations did not participate in the design, execution of the experimental work or writing of this report.

Biochemical Journal (2020) **477** 4491–4513
https://doi.org/10.1042/BCJ20200525

Conflict of interest

The authors declare no conflict of interest.

CRediT Contribution

Sandra Maria Martín Guerrero: Conceptualization, Data curation, Formal analysis, Validation, Investigation, Methodology, Writing — original draft, Writing — review and editing. **Pedro Casado**: Data curation, Formal analysis, Methodology, Writing — review and editing. **Maruan Hijazi**: Formal analysis, Methodology, Writing — review and editing. **Vinothini Rajeeve**: Data curation, Methodology. **Julio Plaza**: Methodology. **Francisco Abadía-Molina**: Writing — review and editing. **Julio Navascués**: Funding acquisition, Writing — review and editing. **Miguel A. Cuadros**: Conceptualization, Writing — original draft, Writing — review and editing. **Pedro R. Cutillas**: Resources, Data curation, Software, Formal analysis, Funding acquisition, Methodology. **David Martín-Oliva**: Conceptualization, Resources, Formal analysis, Supervision, Investigation, Writing — original draft, Writing — review and editing.

Abbreviations

ACC1, acetyl-CoA carboxylase 1; ACN, acetonitrile; AIF, apoptosis-inducing factor; AMOTL1, angiomotin like protein 1; AMPK, AMP-activated protein kinase; ANOVA, one-way analysis of variance; CK1ε/δ, casein-kinase 1; EIF4EBP1, eukaryotic translation initiation factor 4E-binding protein 1; FBS, fetal bovine serum; GO, gene ontology; GPCRs, G-protein-coupled receptors; HCD, higher-energy collisional dissociation; IAM, iodoacetamide; KSEA, kinase substrate enrichment analysis; LARP1, La-related protein 1; LC–MS/MS, liquid chromatography tandem-mass spectrometry; mTOR, mammalian target of rapamycin; MTS, 3-[4,5-dimethylthiazol-2-yl]-2,5-diphenyl tetrazolium bromide; NAFLD, non-alcoholic fatty liver disease; NAMPT, nicotinamide phosphoribosyltransferase; NMN, nicotinamide mononucleotide; NR, nicotinamide riboside; OD, optic density; PAR, poly-ADP-ribose; PARP-1, poly(ADP-ribose) polymerase 1; PARPs, poly(ADP-ribose) polymerases; PFA, paraformaldehyde; ROS, reactive oxygen species; siNT, non-targeting siRNA; siPARP-1, siRNA targeting human PARP-1; siYAP1, siRNA targeting human YAP1; SRB, sulforhodamine B; STIM2, stromal interaction molecule 2; TAZ, transcriptional co-activator with PDZ-binding motifs; TBS/T, tris-buffered saline with 0.1% Tween-20; TFA, trifluoroacetic acid; UGDH, UDP-glucose 6-dehydrogenase; YAP1, yes-associated protein.

References

1 Birben, E., Sahiner, U.M., Sackesen, C., Erzurum, S. and Kalayci, O. (2012) Oxidative stress and antioxidant defense. *World Allergy Organ. J.* **5**, 9–19 https://doi.org/10.1097/WOX.0b013e3182439613
2 Lushchak, V.I. (2014) Free radicals, reactive oxygen species, oxidative stress and its classification. *Chem. Biol. Interact.* **224**, 164–175 https://doi.org/10.1016/j.cbi.2014.10.016
3 Brieger, K., Schiavone, S., Miller, Jr, F.J. and Krause, K.H. (2012) Reactive oxygen species: from health to disease. *Swiss Med. Wkly.* **142**, w13659 https://doi.org/10.4414/smw.2012.13659
4 Rodriguez-Vargas, J.M., Ruiz-Magana, M.J., Ruiz-Ruiz, C., Majuelos-Melguizo, J., Peralta-Leal, A., Rodriguez, M.I. et al. (2012) ROS-induced DNA damage and PARP-1 are required for optimal induction of starvation-induced autophagy. *Cell Res.* **22**, 1181–1198 https://doi.org/10.1038/cr.2012.70
5 Langelier, M.F., Eisemann, T., Riccio, A.A. and Pascal, J.M. (2018) PARP family enzymes: regulation and catalysis of the poly(ADP-ribose) posttranslational modification. *Curr. Opin. Struct. Biol.* **53**, 187–198 https://doi.org/10.1016/j.sbi.2018.11.002
6 Schreiber, V., Dantzer, F., Ame, J.C. and de Murcia, G. (2006) Poly(ADP-ribose): novel functions for an old molecule. nature reviews. *Mol. Cell Biol.* **7**, 517–528 https://doi.org/10.1038/nrm1963
7 Bai, P. (2015) Biology of poly(ADP-Ribose) polymerases: the factotums of cell maintenance. *Mol. Cell* **58**, 947–958 https://doi.org/10.1016/j.molcel.2015.01.034
8 Ha, H.C. and Snyder, S.H. (1999) Poly(ADP-ribose) polymerase is a mediator of necrotic cell death by ATP depletion. *Proc. Natl. Acad. Sci. U.S.A.* **96**, 13978–13982 https://doi.org/10.1073/pnas.96.24.13978
9 Virag, L., Salzman, A.L. and Szabo, C. (1998) Poly(ADP-ribose) synthetase activation mediates mitochondrial injury during oxidant-induced cell death. *J. Immunol.* **161**, 3753–3759 PMID: 9759901
10 Virag, L., Scott, G.S., Cuzzocrea, S., Marmer, D., Salzman, A.L. and Szabo, C. (1998) Peroxynitrite-induced thymocyte apoptosis: the role of caspases and poly (ADP-ribose) synthetase (PARS) activation. *Immunology* **94**, 345–355 https://doi.org/10.1046/j.1365-2567.1998.00534.x
11 Ying, W., Chen, Y., Alano, C.C. and Swanson, R.A. (2002) Tricarboxylic acid cycle substrates prevent PARP-mediated death of neurons and astrocytes. *J. Cereb. Blood Flow Metab.* **22**, 774–779 https://doi.org/10.1097/00004647-200207000-00002
12 Fatokun, A.A., Dawson, V.L. and Dawson, T.M. (2014) Parthanatos: mitochondrial-linked mechanisms and therapeutic opportunities. *Br. J. Pharmacol.* **171**, 2000–2016 https://doi.org/10.1111/bph.12416
13 Jagtap, P. and Szabo, C. (2005) Poly(ADP-ribose) polymerase and the therapeutic effects of its inhibitors. *Nat. Rev. Drug Discov.* **4**, 421–440 https://doi.org/10.1038/nrd1718
14 Slade, D. (2020) PARP and PARG inhibitors in cancer treatment. *Genes Dev.* **34**, 360–394 https://doi.org/10.1101/gad.334516.119

15 Pilie, P.G., Gay, C.M., Byers, L.A., O'Connor, M.J. and Yap, T.A. (2019) PARP inhibitors: extending benefit beyond BRCA-mutant cancers. *Clin. Cancer Res.* **25**, 3759–3771 https://doi.org/10.1158/1078-0432.CCR-18-0968
16 Petr, M.A., Tulika, T., Carmona-Marin, L.M. and Scheibye-Knudsen, M. (2020) Protecting the aging genome. *Trends Cell Biol.* **30**, 117–132 https://doi.org/10.1016/j.tcb.2019.12.001
17 Mao, K., Chen, J., Yu, H., Li, H., Ren, Y., Wu, X. et al. (2020) Poly (ADP-ribose) polymerase 1 inhibition prevents neurodegeneration and promotes alpha-synuclein degradation via transcription factor EB-dependent autophagy in mutant alpha-synucleinA53T model of Parkinson's disease. *Aging Cell* **19**, e13163 https://doi.org/10.1111/acel.13163
18 Martire, S., Mosca, L. and d'Erme, M. (2015) PARP-1 involvement in neurodegeneration: a focus on Alzheimer's and Parkinson's diseases. *Mech. Ageing Dev.* **146-148**, 53–64 https://doi.org/10.1016/j.mad.2015.04.001
19 Mouchiroud, L., Houtkooper, R.H., Moullan, N., Katsyuba, E., Ryu, D., Canto, C. et al. (2013) The NAD(+)/Sirtuin pathway modulates longevity through activation of mitochondrial UPR and FOXO signaling. *Cell* **154**, 430–441 https://doi.org/10.1016/j.cell.2013.06.016
20 Pan, D. (2010) The hippo signaling pathway in development and cancer. *Dev. Cell* **19**, 491–505 https://doi.org/10.1016/j.devcel.2010.09.011
21 Zhao, B., Wei, X., Li, W., Udan, R.S., Yang, Q., Kim, J. et al. (2007) Inactivation of YAP oncoprotein by the Hippo pathway is involved in cell contact inhibition and tissue growth control. *Genes Dev.* **21**, 2747–2761 https://doi.org/10.1101/gad.1602907
22 Zhao, B., Li, L., Tumaneng, K., Wang, C.Y. and Guan, K.L. (2010) A coordinated phosphorylation by Lats and CK1 regulates YAP stability through SCF (beta-TRCP). *Genes Dev.* **24**, 72–85 https://doi.org/10.1101/gad.1843810
23 Liu, C.Y., Zha, Z.Y., Zhou, X., Zhang, H., Huang, W., Zhao, D. et al. (2010) The hippo tumor pathway promotes TAZ degradation by phosphorylating a phosphodegron and recruiting the SCF{beta}-TrCP E3 ligase. *J. Biol. Chem.* **285**, 37159–37169 https://doi.org/10.1074/jbc.M110.152942
24 Zhao, B., Ye, X., Yu, J., Li, L., Li, W., Li, S. et al. (2008) TEAD mediates YAP-dependent gene induction and growth control. *Genes Dev.* **22**, 1962–1971 https://doi.org/10.1101/gad.1664408
25 Zhao, Y. and Yang, X. (2015) Regulation of sensitivity of tumor cells to antitubulin drugs by Cdk1-TAZ signalling. *Oncotarget* **6**, 21906–21917 https://doi.org/10.18632/oncotarget.4259
26 Meng, Z., Moroishi, T. and Guan, K.L. (2016) Mechanisms of Hippo pathway regulation. *Genes Dev.* **30**, 1–17 https://doi.org/10.1101/gad.274027.115
27 Mao, B., Gao, Y., Bai, Y. and Yuan, Z. (2015) Hippo signaling in stress response and homeostasis maintenance. *Acta Biochim. Biophys. Sin. (Shanghai)* **47**, 2–9 https://doi.org/10.1093/abbs/gmu109
28 Wang, Y., Yu, A. and Yu, F.X. (2017) The Hippo pathway in tissue homeostasis and regeneration. *Protein Cell* **8**, 349–359 https://doi.org/10.1007/s13238-017-0371-0
29 Moroishi, T., Hansen, C.G. and Guan, K.L. (2015) The emerging roles of YAP and TAZ in cancer. *Nat. Rev. Cancer* **15**, 73–79 https://doi.org/10.1038/nrc3876
30 Martin-Guerrero, S.M., Munoz-Gamez, J.A., Carrasco, M.C., Salmeron, J., Martin-Estebane, M., Cuadros, M.A. et al. (2017) Poly(ADP-ribose) polymerases inhibitors prevent early mitochondrial fragmentation and hepatocyte cell death induced by H2O2. *PLoS One* **12**, e0187130 https://doi.org/10.1371/journal.pone.0187130
31 Vichai, V. and Kirtikara, K. (2006) Sulforhodamine B colorimetric assay for cytotoxicity screening. *Nat. Protoc.* **1**, 1112–1116 https://doi.org/10.1038/nprot.2006.179
32 Casado, P., Wilkes, E.H., Miraki-Moud, F., Hadi, M.M., Rio-Machin, A., Rajeeve, V. et al. (2018) Proteomic and genomic integration identifies kinase and differentiation determinants of kinase inhibitor sensitivity in leukemia cells. *Leukemia* **32**, 1818–1822 https://doi.org/10.1038/s41375-018-0032-1
33 Martin-Guerrero, S.M., Casado, P., Munoz-Gamez, J.A., Carrasco, M.C., Navascues, J., Cuadros, M.A. et al. (2019) Poly(ADP-Ribose) polymerase-1 inhibition potentiates cell death and phosphorylation of DNA damage response proteins in oxidative stressed retinal cells. *Exp. Eye Res.* **188**, 107790 https://doi.org/10.1016/j.exer.2019.107790
34 Arnandis, T., Monteiro, P., Adams, S.D., Bridgeman, V.L., Rajeeve, V., Gadaleta, E. et al. (2018) Oxidative stress in cells with extra centrosomes drives non-cell-autonomous invasion. *Dev. Cell* **47**, 409–424.e409 https://doi.org/10.1016/j.devcel.2018.10.026
35 Perkins, D.N., Pappin, D.J., Creasy, D.M. and Cottrell, J.S. (1999) Probability-based protein identification by searching sequence databases using mass spectrometry data. *Electrophoresis* **20**, 3551–3567 https://doi.org/10.1002/(SICI)1522-2683(19991201)20:18<3551::AID-ELPS3551>3.0.CO;2-2
36 Casado, P., Rodriguez-Prados, J.C., Cosulich, S.C., Guichard, S., Vanhaesebroeck, B., Joel, S. et al. (2013) Kinase-substrate enrichment analysis provides insights into the heterogeneity of signaling pathway activation in leukemia cells. *Sci. Signal.* **6**, rs6 https://doi.org/10.1126/scisignal.2003573
37 Babicki, S., Arndt, D., Marcu, A., Liang, Y., Grant, J.R., Maciejewski, A. et al. (2016) Heatmapper: web-enabled heat mapping for all. *Nucleic Acids Res.* **44**, W147–W153 https://doi.org/10.1093/nar/gkw419
38 Huang da, W., Sherman, B.T. and Lempicki, R.A. (2009) Systematic and integrative analysis of large gene lists using DAVID bioinformatics resources. *Nat. Protoc.* **4**, 44–57 https://doi.org/10.1038/nprot.2008.211
39 Wegrowski, Y. and Pitsillides, A.A. (2014) UDP-glucose 6-dehydrogenase (UGDH). In *Handbook of Glycosyltransferases and Related Genes* (Taniguchi, N., Honke, K., Fukuda, M., Narimatsu, H., Yamaguchi, Y. and Angata, T., eds.), pp. 1425–1437, Springer, Tokyo, Japan
40 Soboloff, J., Madesh, M. and Gill, D.L. (2011) Sensing cellular stress through STIM proteins. *Nat. Chem. Biol.* **7**, 488–492 https://doi.org/10.1038/nchembio.619
41 Manmadhan, S. and Ehmer, U. (2019) Hippo signaling in the liver - a long and ever-expanding story. *Front. Cell Dev. Biol.* **7**, 33 https://doi.org/10.3389/fcell.2019.00033
42 Kodaka, M. and Hata, Y. (2015) The mammalian Hippo pathway: regulation and function of YAP1 and TAZ. *Cell. Mol. Life Sci.* **72**, 285–306 https://doi.org/10.1007/s00018-014-1742-9
43 Wei, J., Zhang, Y., Yu, T.Y., Sadre-Bazzaz, K., Rudolph, M.J., Amodeo, G.A. et al. (2016) A unified molecular mechanism for the regulation of acetyl-CoA carboxylase by phosphorylation. *Cell Discov.* **2**, 16044 https://doi.org/10.1038/celldisc.2016.44
44 Treebak, J.T., Pehmoller, C., Kristensen, J.M., Kjobsted, R., Birk, J.B., Schjerling, P. et al. (2014) Acute exercise and physiological insulin induce distinct phosphorylation signatures on TBC1D1 and TBC1D4 proteins in human skeletal muscle. *J. Physiol.* **592**, 351–375 https://doi.org/10.1113/jphysiol.2013.266338
45 Fonseca, B.D., Lahr, R.M., Damgaard, C.K., Alain, T. and Berman, A.J. (2018) LARP1 on TOP of ribosome production. *Wiley Interdiscip. Rev. RNA* **9**, e1480 https://doi.org/10.1002/wrna.1480

Biochemical Journal (2020) **477** 4491–4513
https://doi.org/10.1042/BCJ20200525

46 Qin, X., Jiang, B. and Zhang, Y. (2016) 4E-BP1, a multifactor regulated multifunctional protein. *Cell Cycle* **15**, 781–786 https://doi.org/10.1080/15384101.2016.1151581

47 Garcia, D. and Shaw, R.J. (2017) AMPK: mechanisms of cellular energy sensing and restoration of metabolic balance. *Mol. Cell* **66**, 789–800 https://doi.org/10.1016/j.molcel.2017.05.032

48 Alano, C.C., Garnier, P., Ying, W., Higashi, Y., Kauppinen, T.M. and Swanson, R.A. (2010) NAD+ depletion is necessary and sufficient for poly (ADP-ribose) polymerase-1-mediated neuronal death. *J. Neurosci.* **30**, 2967–2978 https://doi.org/10.1523/JNEUROSCI.5552-09.2010

49 Mester, L., Szabo, A., Atlasz, T., Szabadfi, K., Reglodi, D., Kiss, P. et al. (2009) Protection against chronic hypoperfusion-induced retinal neurodegeneration by PARP inhibition via activation of PI-3-kinase Akt pathway and suppression of JNK and p38 MAP kinases. *Neurotox. Res.* **16**, 68–76 https://doi.org/10.1007/s12640-009-9049-6

50 Xu, Y., Huang, S., Liu, Z.G. and Han, J. (2006) Poly(ADP-ribose) polymerase-1 signaling to mitochondria in necrotic cell death requires RIP1/TRAF2-mediated JNK1 activation. *J. Biol. Chem.* **281**, 8788–8795 https://doi.org/10.1074/jbc.M508135200

51 Kraus, W.L. and Lis, J.T. (2003) PARP goes transcription. *Cell* **113**, 677–683 https://doi.org/10.1016/S0092-8674(03)00433-1

52 Izhar, L., Adamson, B., Ciccia, A., Lewis, J., Pontano-Vaites, L., Leng, Y. et al. (2015) A systematic analysis of factors localized to damaged chromatin reveals PARP-dependent recruitment of transcription factors. *Cell Rep.* **11**, 1486–1500 https://doi.org/10.1016/j.celrep.2015.04.053

53 Hocsak, E., Szabo, V., Kalman, N., Antus, C., Cseh, A., Sumegi, K. et al. (2017) PARP inhibition protects mitochondria and reduces ROS production via PARP-1-ATF4-MKP-1-MAPK retrograde pathway. *Free Radic. Biol. Med.* **108**, 770–784 https://doi.org/10.1016/j.freeradbiomed.2017.04.018

54 Yu, F.X., Zhao, B. and Guan, K.L. (2015) Hippo pathway in organ size control, tissue homeostasis, and cancer. *Cell* **163**, 811–828 https://doi.org/10.1016/j.cell.2015.10.044

55 Shao, D., Zhai, P., Del Re, D.P., Sciarretta, S., Yabuta, N., Nojima, H. et al. (2014) A functional interaction between Hippo-YAP signalling and FoxO1 mediates the oxidative stress response. *Nat. Commun.* **5**, 3315 https://doi.org/10.1038/ncomms4315

56 Del Re, D.P., Yang, Y., Nakano, N., Cho, J., Zhai, P., Yamamoto, T. et al. (2013) Yes-associated protein isoform 1 (Yap1) promotes cardiomyocyte survival and growth to protect against myocardial ischemic injury. *J. Biol. Chem.* **288**, 3977–3988 https://doi.org/10.1074/jbc.M112.436311

57 LaCanna, R., Liccardo, D., Zhang, P., Tragesser, L., Wang, Y., Cao, T. et al. (2019) Yap/Taz regulate alveolar regeneration and resolution of lung inflammation. *J. Clin. Invest.* **129**, 2107–2122 https://doi.org/10.1172/JCI125014

58 Grijalva, J.L., Huizenga, M., Mueller, K., Rodriguez, S., Brazzo, J., Camargo, F. et al. (2014) Dynamic alterations in Hippo signaling pathway and YAP activation during liver regeneration. *Am. J. Physiol. Gastrointest. Liver Physiol.* **307**, G196–G204 https://doi.org/10.1152/ajpgi.00077.2014

59 Liu, Y., Lu, T., Zhang, C., Xu, J., Xue, Z., Busuttil, R.W. et al. (2019) Activation of YAP attenuates hepatic damage and fibrosis in liver ischemia-reperfusion injury. *J. Hepatol.* **71**, 719–730 https://doi.org/10.1016/j.jhep.2019.05.029

60 Lu, L., Finegold, M.J. and Johnson, R.L. (2018) Hippo pathway coactivators Yap and Taz are required to coordinate mammalian liver regeneration. *Exp. Mol. Med.* **50**, e423 https://doi.org/10.1038/emm.2017.205

61 Oh, S.H., Swiderska-Syn, M., Jewell, M.L., Premont, R.T. and Diehl, A.M. (2018) Liver regeneration requires Yap1-TGFbeta-dependent epithelial-mesenchymal transition in hepatocytes. *J. Hepatol.* **69**, 359–367 https://doi.org/10.1016/j.jhep.2018.05.008

62 Tharehalli, U., Svinarenko, M., Kraus, J.M., Kuhlwein, S.D., Szekely, R., Kiesle, U. et al. (2018) YAP activation drives liver regeneration after cholestatic damage induced by Rbpj deletion. *Int. J. Mol. Sci.* **19**, 3801 https://doi.org/10.3390/ijms19123801

63 Chen, J., You, H., Li, Y., Xu, Y., He, Q. and Harris, R.C. (2018) EGF receptor-dependent YAP activation is important for renal recovery from AKI. *J. Am. Soc. Nephrol.* **29**, 2372–2385 https://doi.org/10.1681/ASN.2017121272

64 Javle, M. and Curtin, N.J. (2011) The role of PARP in DNA repair and its therapeutic exploitation. *Br. J. Cancer* **105**, 1114–1122 https://doi.org/10.1038/bjc.2011.382

65 Virag, L., Salzman, A.L. and Szabo, C. (1998) Poly(ADP-ribose) synthetase activation mediates mitochondrial injury during oxidant-induced cell death. *J. Immunol.* **161**, 3753–3759 PMID: 9759901

66 Diani-Moore, S., Shoots, J., Singh, R., Zuk, J.B. and Rifkind, A.B. (2017) NAD(+) loss, a new player in AhR biology: prevention of thymus atrophy and hepatosteatosis by NAD(+) repletion. *Sci. Rep.* **7**, 2268 https://doi.org/10.1038/s41598-017-02332-9

67 Zhu, Y., Zhao, K.-K., Tong, Y., Zhou, Y.-L., Wang, Y.-X., Zhao, P.-Q. et al. (2016) Exogenous NAD(+) decreases oxidative stress and protects H_2O_2-treated RPE cells against necrotic death through the up-regulation of autophagy. *Sci. Rep.* **6**, 26322 https://doi.org/10.1038/srep26322

68 Griffiths, H.B.S., Williams, C., King, S.J. and Allison, S.J. (2020) Nicotinamide adenine dinucleotide (NAD+): essential redox metabolite, co-substrate and an anti-cancer and anti-ageing therapeutic target. *Biochem. Soc. Trans.* **48**, 733–744 https://doi.org/10.1042/BST20190033

69 Johnson, S. and Imai, S.I. (2018) NAD (+) biosynthesis, aging, and disease. *F1000Res* **7**, 132 https://doi.org/10.12688/f1000research.12120.1

70 Yoshino, J., Mills, K.F., Yoon, M.J. and Imai, S. (2011) Nicotinamide mononucleotide, a key NAD(+) intermediate, treats the pathophysiology of diet- and age-induced diabetes in mice. *Cell Metab.* **14**, 528–536 https://doi.org/10.1016/j.cmet.2011.08.014

71 Stein, L.R. and Imai, S. (2014) Specific ablation of Nampt in adult neural stem cells recapitulates their functional defects during aging. *EMBO J.* **33**, 1321–1340 https://doi.org/10.1002/embj.201386917

72 Yaku, K., Okabe, K., Hikosaka, K. and Nakagawa, T. (2018) NAD metabolism in cancer therapeutics. *Front. Oncol.* **8**, 622 https://doi.org/10.3389/fonc.2018.00622

73 Meng, Y.Y., Wu, C.W., Yu, B., Li, H., Chen, M. and Qi, G.X. (2018) PARP-1 Involvement in autophagy and their roles in apoptosis of vascular smooth muscle cells under oxidative stress. *Folia Biol.* **64**, 103–111 PMID: 30394268

74 Virag, L., Robaszkiewicz, A., Rodriguez-Vargas, J.M. and Oliver, F.J. (2013) Poly(ADP-ribose) signaling in cell death. *Mol. Asp. Med.* **34**, 1153–1167 https://doi.org/10.1016/j.mam.2013.01.007

75 Ethier, C., Tardif, M., Arul, L. and Poirier, G.G. (2012) PARP-1 modulation of mTOR signaling in response to a DNA alkylating agent. *PLoS One* **7**, e47978 https://doi.org/10.1371/journal.pone.0047978

76 Mo, J.S., Meng, Z., Kim, Y.C., Park, H.W., Hansen, C.G., Kim, S. et al. (2015) Cellular energy stress induces AMPK-mediated regulation of YAP and the Hippo pathway. *Nat. Cell Biol.* **17**, 500–510 https://doi.org/10.1038/ncb3111

77 DeRan, M., Yang, J., Shen, C.H., Peters, E.C., Fitamant, J., Chan, P. et al. (2014) Energy stress regulates hippo-YAP signaling involving AMPK-mediated regulation of angiomotin-like 1 protein. *Cell Rep.* **9**, 495–503 https://doi.org/10.1016/j.celrep.2014.09.036

78 Wang, W., Xiao, Z.D., Li, X., Aziz, K.E., Gan, B., Johnson, R.L. et al. (2015) AMPK modulates Hippo pathway activity to regulate energy homeostasis. *Nat. Cell Biol.* **17**, 490–499 https://doi.org/10.1038/ncb3113
79 Masarone, M., Rosato, V., Dallio, M., Gravina, A.G., Aglitti, A., Loguercio, C. et al. (2018) Role of oxidative stress in pathophysiology of nonalcoholic fatty liver disease. *Oxidative Med. Cell. Longev.* **2018**, 9547613 https://doi.org/10.1155/2018/9547613
80 Huang, K., Du, M., Tan, X., Yang, L., Li, X., Jiang, Y. et al. (2017) PARP1-mediated PPARalpha poly(ADP-ribosyl)ation suppresses fatty acid oxidation in non-alcoholic fatty liver disease. *J. Hepatol.* **66**, 962–977 https://doi.org/10.1016/j.jhep.2016.11.020
81 Wattacheril, J., Rose, K.L., Hill, S., Lanciault, C., Murray, C.R., Washington, K. et al. (2017) Non-alcoholic fatty liver disease phosphoproteomics: A functional piece of the precision puzzle. *Hepatol. Res.* **47**, 1469–1483 https://doi.org/10.1111/hepr.12885
82 Perez-Riverol, Y., Csordas, A., Bai, J., Bernal-Llinares, M., Hewapathirana, S., Kundu, D.J. et al. (2019) The PRIDE database and related tools and resources in 2019: improving support for quantification data. *Nucleic Acids Res.* **47**, D442–D450 https://doi.org/10.1093/nar/gky1106